Development of an algebraic-closure-based moment method for unsteady Eulerian simulations of particle-laden turbulent flows in very dilute regime

E. Masi [a,b,*], O. Simonin [a,b], E. Riber [c], P. Sierra [c], L.Y.M. Gicquel [c]

[a] Université de Toulouse, INPT, UPS, IMFT (Institut de Mécanique des Fluides de Toulouse), Allée Camille Soula, F-31400 Toulouse, France
[b] CNRS, IMFT, F-31400 Toulouse, France
[c] CERFACS, 42 avenue Gaspard Coriolis, 31057 Toulouse Cédex 1, France

Keywords:
PDF method
Moment approach
Two-fluid model for DNS/LES
RUM particle kinetic stress tensor

A B S T R A C T

An algebraic-closure-based moment method (ACBMM) is developed for unsteady Eulerian particle simulations, coupled with direct numerical simulations (DNSs) of fluid turbulent flows, in very dilute regime and up to large Stokes numbers St_K (based on the Kolmogorov timescale) or moderate Stokes numbers St (based on the turbulent macroscale seen by the particles). The proposed method is developed in the frame of a conditional statistical approach which provides a local and instantaneous characterization of the dispersed-phase dynamic accounting for the effect of crossing between particle trajectories which becomes substantial for $St_K > 1$. The computed Eulerian quantities are low-order moments of the conditional probability density function (PDF) and the corresponding governing equations are derived from the PDF kinetic equation in the general frame of the kinetic theory of gases. At the first order, the computation of the mesoscopic particle number density and velocity requires the modeling of the second-order moment tensor appearing in the particle momentum equation and referred to as random uncorrelated motion (RUM) particle kinetic stress tensor. The current work proposes a variety of different algebraic closures for the deviatoric part of the tensor. An evaluation of some effective propositions is given by performing an *a priori* analysis using particle Eulerian fields which are extracted from particle Lagrangian simulations coupled with DNS of a temporal particle-laden turbulent planar jet. Several million-particle simulations are analyzed in order to assess the models for various Stokes numbers. It is apparent that the most fruitful are explicit algebraic stress models (2ΦEASM) which are based on an equilibrium assumption of RUM anisotropy for which explicit solutions are provided by means of a polynomial representation for tensor functions. These models compare very well with Eulerian–Lagrangian DNSs and properly represent all crucial trends extracted from such simulations.

1. Introduction

1.1. Overview: Lagrangian versus Eulerian approaches

Dilute particle/droplet-laden turbulent flows are of central importance in many industrial applications as, for example, in combustion chambers of aeronautic engines or recirculating fluidized beds in chemical engineering. The highly-turbulent unsteady nature of these mixtures, in most cases confined in complex geometries, increases the complexity of their predictions and the modeling is still a challenge nowadays. In order for a model to be appropriate, two requirements must be satisfied: (i) the approach must be sufficiently accurate for providing right predictions in such complex situations and (ii) it must be usable for real applications at industrial scale. In very dilute regime, and for mixtures of interest to this study, particles have size smaller or comparable to the smallest lengthscale of the turbulence and the volume fraction and the mass loading of the dispersed phase are small enough to neglect collisions and turbulence modulation. For these flows, for which a point-particle approximation applies, the Eulerian–Lagrangian direct-numerical-simulation (DNS) approach is an uncontroversial accurate method. DNSs of the fluid turbulence are straightforwardly coupled with Lagrangian particle simulations by accurate interpolation of the fluid properties at the particle location (Riley and Paterson, 1974). The Eulerian–Lagrangian DNS method does not require further modeling efforts and it is easy to implement in existing single-phase DNS codes. For this reason, it has been extensively used over the years and nowadays it is considered as a reference when experimental data are not available. However, this approach is unfeasible in most real cases and its

* Corresponding author at: IMFT (Institut de Mécanique des Fluides de Toulouse), Allée Camille Soula, F-31400 Toulouse, France.
E-mail address: emasi@imft.fr (E. Masi).

http://dx.doi.org/10.1016/j.ijmultiphaseflow.2013.10.001

use unrealistic at industrial scale. For industrial applications the constraint is double: the computational cost of the DNS for such flows is prohibitively expensive; realistic industrial flow configurations involve a huge number of particles which, according to the Lagrangian method, have to be tracked separately with a consequent increase of computational costs. An alternative method for predicting unsteady turbulent particle-laden flows with a high level of accuracy is the Eulerian–Eulerian large-eddy simulation (LES) approach. This method seems indeed fulfill the two aforementioned requirements of high accuracy and reasonable computational cost (the reader is referred to Fox (2012) for a review about the LES approaches in multiphase flows).

In the Eulerian–Eulerian approach, the particles are described in an Eulerian framework as a continuous medium, and the two-phase governing equations are solved separately but coupled through interphase exchange terms. In the literature, several successful Eulerian models have been proposed to predict the dispersion of particles when the turbulence is modeled by using Reynolds-averaged Navier–Stokes (RANS) methods. Among these, we recall the phase-averaging (Elghobashi and Abou-Arab, 1983; Chen and Wood, 1985; Zhou, 2010) and the probability density function (PDF) (Reeks, 1991; Simonin, 1991a; Zaichik and Vinberg, 1991) approaches. As pointed out by Balzer et al. (1996), such PDF approaches are formally consistent with particulate Eulerian models based on the granular kinetic theory, which are extensively used in dense gas–solid flows when the particle dynamics is dominated by the particle–particle or the particle–wall collisions (see, e.g Gidaspow, 1994). In contrast, the unsteady (DNS/LES) Eulerian modeling of dilute particulate flows is a timely topic of research. In this paper we will focus on the unsteady Eulerian–Eulerian DNS approach as the baseline of the Eulerian–Eulerian LES approach (Moreau et al., 2010). The modeling suggested by this work should not be confused with the aforementioned two-fluid RANS approaches. Some unsteady (DNS) Eulerian models available in the literature are instead recalled below.

A local Eulerian characterization of the dispersed phase was suggested by Maxey (1987) who using a Taylor expansion of the particle-motion equation in powers of Stokes number provided an expression for the particle-velocity field in terms of fluid velocity and its derivatives. In this approximation, only one equation for the particle concentration must be resolved and the dispersed phase would not require additional modeling. This approach was extended by Ferry and Balachandar (2001) in order to account for the added mass, Saffman lift and Basset history forces and evaluated by DNSs of homogeneous isotropic turbulence (HIT) (Rani and Balachandar, 2003) and homogeneous turbulent mean-sheared flows (Shotorban and Balachandar, 2006). In the literature, it is often referred to as equilibrium Eulerian approach or fast Eulerian method. Successfully assessed for small particle inertia, this approach fails for Stokes numbers, based on the Kolmogorov lengthscale, St_K, approaching unity (Rani and Balachandar, 2003; Shotorban and Balachandar, 2006). An alternative unsteady approach was suggested by Druzhinin (1995) who used a spatial average of the particle equations over a lenghtscale much greater than the particle diameter and of the order of the smallest lenghtscale of the flow. The resulting system of closed Eulerian equations for the particle volume fraction and the particle velocity was tested in DNSs of particle-laden circular vortex and HIT of bubbles and particles, in one-way and two-way coupling (Druzhinin and Elghobashi, 1998, 1999). In the frame of the modeling of polydispersed flows, we also recall the multi-fluid method of Laurent and Massot (2001), which assumes a monokinetic description of the particle velocity. Also these approaches are restricted to small particle inertia. For large Stokes numbers, alternative effective models are described in Sections 1.2 and 1.3.

1.2. An unsteady Eulerian approach for large Stokes numbers

Recently, Février et al. (2005) showed that in order for an Eulerian approach to be able to model the dispersed phase composed of particles having response times larger than the Kolmogorov timescale, it should account for the effect of crossing between particle trajectories. This effect involves many different velocities in the same volume of control violating the assumption of the uniqueness of the particle velocity distribution. By introducing a new operator of ensemble average over a large number of particle realizations conditional on a given fluid flow realization, local statistics of the dispersed phase may be derived in the framework of the conditional PDF approach. The novel conditional statistical approach (Février et al., 2005), known as mesoscopic Eulerian formalism (MEF), is based on the idea that the particle velocity may be partitioned in two contributions: (i) an Eulerian particle velocity field, referred to as mesoscopic field, which is spatially correlated and shared by all the particles and which accounts for correlations between particles and between particles and fluid and (ii) a spatially-uncorrelated particle velocity component, referred to as random uncorrelated motion (RUM) contribution, associated with each particle and resulting from the chaotic particles' behavior. In the Eulerian transport equations, the RUM contribution is characterized in terms of Eulerian fields of particle velocity moments; the larger is the particle inertia the more important is RUM. According to MEF, the assumption of the uniqueness of the particle velocity distribution is no longer a constraint since this model accounts separately for correlated and chaotic contributions which characterize the particle velocity property at large Stokes numbers. The existence of a spatially-uncorrelated velocity due to the crossing of particle trajectories was already pointed out by Falkovich et al. (2002); modeling this contribution is crucial in order for an Eulerian model to be effective in dilute regime. In the literature, MEF was used by IJzermans et al. (2010) and Meneguz and Reeks (2011) for characterizing the particle segregation by a full Lagrangian method (FLM) and by Gustavsson et al. (2012) who analyzed the relationship between caustics, singularities and RUM. Vance et al. (2006) used MEF to investigate the spatial characteristics of the particle velocity field in a turbulent channel flow with and without inter-particle collisions. Simonin et al. (2006) compared such an approach with a two-point PDF method (Zaichik et al., 2003), pointing out the ability of the latter to capture the behavior of the dispersed phase as modeled by the MEF decomposition. In this study, we will use the conditional PDF approach in the framework of a moment method and we will focus on the closures of the system of equations derived from.

1.3. The conditional PDF approach and the question of the closures

According to the conditional PDF approach (described in Section 2), the PDF kinetic equation is closed at the same level than the Lagrangian equation governing the discrete particle variables, such as the drag law formulation in the dynamic equation. Unfortunately, a closed kinetic equation for the PDF does not completely solve the closure problem since this evolution equation in phase space creates an infinite set of coupled moment equations in real space. So any finite set of moment equations has to be supplemented by closure models of the unknown moments written in terms of the computed ones. Depending on the closure, models may be provided by using a Grad's moment method (Grad, 1949) or by means of quadrature-based moment methods (QBMMs) or kinetic-based-moment methods (KBMMs) (McGraw, 1997; Marchisio and Fox, 2005; Fox, 2008; Fox et al., 2008; Desjardins et al., 2008; Passalacqua et al., 2010; Kah et al., 2010; Yuan and Fox, 2011; Vié et al., 2011; Chalons et al., 2012). Grad's, QBMM

and KBMM approaches rely on a presumed PDF written in the phase space; mathematical arguments are then used in order to address the closure question. These methods are particularly interesting since their mathematical formulation of the problem does not require further efforts about the formulation of physical assumptions needed for modeling the closures. However, they may require a large number of moments in order to converge toward an accurate solution if the shape of the presumed PDF is not sufficiently close to that of the actual PDF, with the consequence that additional high-order-moment transport equations could be necessary. This would involve additional costs which must be considered when modeling fully unsteady three-dimensional turbulent flows in realistic configurations.

An alternative is to close the unknown higher-order moments by using algebraic closures derived by analogy with the kinetic theory or with turbulence models. Hereinafter, we will refer to this approach as ACBMM (algebraic-closure-based moment method). Contrary to QBMM/KBMM or Grad's methods, ACBMM is a semi-empirical model derived directly in the physical space. In isothermal conditions, Simonin et al. (2002) and Kaufmann et al. (2008) suggested an ACBMM in which the transport equations of the low-order moments (the particle number density and the particle mesoscopic velocity) are numerically solved. The second-order moment appearing in the particle momentum equation, the RUM particle kinetic stress tensor, is closed by solving an additional equation for its isotropic part and by using a viscosity assumption for the deviatoric part. The timescale involved in the viscosity modeling is the particle response time. The appropriateness of such a closure is investigated by the present work. ACBMM has then been used to derive the Eulerian–Eulerian LES modeling (Moreau et al., 2010) in order to predict accurate unsteady particle-laden turbulent flows in more realistic situations as, for instance, in complex geometries (Riber et al., 2009). Indeed, the originality of the ACBMM approach comes out in the framework of the LES modeling. Using the partitioning of the particle velocity in two contributions makes it possible to separate quantities which are intrinsically different as they stem from interactions with different scales of the turbulence. Moments of these contributions show different scaling laws when spatially filtered (Moreau, 2006) which means that they need to be modeled separately. Recently, MEF was extended to non-isothermal conditions and ACBMM used to model evaporating droplet-laden turbulent flows (Masi et al., 2011).

1.4. Objective

So far, the ACBMM using the aforementioned algebraic closure based on a standard viscosity assumption has shown to be able to predict particle-laden HIT (Kaufmann et al., 2008) at moderate Stokes numbers, St_K. In the meantime and while performing preliminary *a posteriori* tests (Riber, 2007) in mean-sheared flow conditions and large Stokes numbers, this approach failed. The reason must be sought in the failure of the viscosity assumption which is no longer able to predict the RUM stress tensor in such conditions. In very dilute regime in which the particle velocity distribution can be far from equilibrium, such an assumption seems indeed questionable, especially in the presence of a mean shear and large Stokes numbers. The aim of this work is to address the concern of the algebraic closure of the RUM stress tensor in order to enable ACBMM to successfully predicts the unsteady dispersed phase in mean-sheared turbulent flows and large Stokes numbers as well.

The manuscript is organized as follows. In Section 2 the unsteady Eulerian statistical approach and the local and instantaneous particle Eulerian equations are presented. At the first order, the equation system needs a closure for the RUM particle kinetic stress tensor. In order to provide such a closure, which relies on a relationship between the RUM and the particle rate-of-strain tensors, in Section 3 the two tensors are described and a previous analysis about their structure is recalled. Finally, several algebraic closures are proposed and presented in Section 4. They are developed by means of some techniques used in turbulence for closing the one-point second-order velocity moments. Eulerian–Lagrangian DNS and the methodology adopted for the *a priori* analysis are described in Section 5. From the Eulerian particle database extracted from the Lagrangian particle data, the closures developed by the present study are assessed. Results of the assessment are presented in Section 6. Summary and conclusions are given in Section 7.

2. Unsteady Eulerian statistical approach for the inertial dispersed phase

In this section, the conditional PDF approach (Février et al., 2005) as well as the local and instantaneous Eulerian equations of the dispersed phase are briefly presented; they will be used in the framework of the ACBMM approach.

2.1. The conditional PDF approach

The dispersed phase is described in terms of a conditional PDF. The statistical approach uses ensemble averages over a large number $\mathcal{N}_p$ of particulate phase realizations $\mathcal{H}_p$, slightly differing in their initial conditions, conditional on one-fluid flow realization $\mathcal{H}_f$. According to this formalism, information concerning spatial and/or temporal correlations between particles are maintained. In dilute regime where there is neither turbulence modulation nor inter-particle interactions, the one-particle conditional PDF provides a complete description of the particle spatially-correlated motion. It is defined as

$$\tilde{f}_p^{(1)}(\boldsymbol{x},\boldsymbol{c}_p,t;\mathcal{H}_f)=\lim_{\mathcal{N}_p\to\infty}\left[\frac{1}{\mathcal{N}_p}\sum_{\mathcal{N}_p}\sum_{m=1}^{N_p}W_p^{(m)}(\boldsymbol{x},\boldsymbol{c}_p,t;\mathcal{H}_p,\mathcal{H}_f)\right], \tag{1}$$

with N_p the whole particle number of any realization and $W_p^{(m)}(\boldsymbol{x},\boldsymbol{c}_p,t;\mathcal{H}_p,\mathcal{H}_f)=\delta(\boldsymbol{x}-\boldsymbol{x}_p^{(m)}(t))\delta(\boldsymbol{c}_p-\boldsymbol{u}_p^{(m)}(t))$ the refined-grid density (Reeks, 1991) accounting for particles with centre $\boldsymbol{x}_p$ located in the volume $[\boldsymbol{x},\boldsymbol{x}+\delta\boldsymbol{x}]$ and translation velocity $\boldsymbol{u}_p$ in $[\boldsymbol{c}_p,\boldsymbol{c}_p+\delta\boldsymbol{c}_p]$, at the time t. The mesoscopic average of any Lagrangian quantity $\mathbf{g}_p(t)$ which can be written as a function of the particle velocity, $\mathbf{g}_p(t)=\boldsymbol{\gamma}(\boldsymbol{u}_p(t))$, is obtained by integration over the particle velocity space leading to the mesoscopic field variable $\tilde{\mathbf{g}}_p(\boldsymbol{x},t)$ as

$$\tilde{\mathbf{g}}_p(\boldsymbol{x},t)=\frac{1}{\tilde{n}_p(\boldsymbol{x},t)}\int\boldsymbol{\gamma}(\boldsymbol{c}_p)\tilde{f}_p^{(1)}(\boldsymbol{x},\boldsymbol{c}_p,t;\mathcal{H}_f)d\boldsymbol{c}_p, \tag{2}$$

where $\tilde{n}_p$ is the mesoscopic particle number density obtained by the integration of $\tilde{f}_p^{(1)}$. Hereinafter, for the sake of synthesis, the contracted notation $\tilde{\mathbf{g}}_p(\boldsymbol{x},t)=\langle\mathbf{g}_p(t)|\boldsymbol{x}_p(t)=\boldsymbol{x};\mathcal{H}_f\rangle=\langle\mathbf{g}_p(t)|\mathcal{H}_f\rangle_p$ is used. From the latter it is possible to write the macroscopic particle properties, obtained by the standard ensemble averaging on turbulent two-phase realizations derived in the frame of the RANS approach (see, e.g. Simonin, 2000) as

$$\langle\cdot\rangle_p=\frac{1}{n_p(\boldsymbol{x},t)}\lim_{\mathcal{N}_f\to\infty}\frac{1}{\mathcal{N}_f}\sum_{\mathcal{N}_f}\tilde{n}_p(\boldsymbol{x},t)\langle\cdot|\mathcal{H}_f\rangle_p, \tag{3}$$

which corresponds to the standard, i.e. no longer conditional, one-particle PDF

$$f_p^{(1)}(\boldsymbol{x},\boldsymbol{c}_p,t)=\lim_{\mathcal{N}_f,\mathcal{N}_p\to\infty}\left[\frac{1}{\mathcal{N}_f}\sum_{\mathcal{N}_f}\left[\frac{1}{\mathcal{N}_p}\sum_{\mathcal{N}_p}\sum_{m=1}^{N_p}W_p^{(m)}(\boldsymbol{x},\boldsymbol{c}_p,t;\mathcal{H}_p,\mathcal{H}_f)\right]\right]. \tag{4}$$

The macroscopic average $\mathbf{G}_p(\boldsymbol{x},t)$ of any Lagrangian property $\mathbf{g}_p(t)$ can be directly linked to the ensemble average of the mesoscopic variable on the fluid turbulent realizations as

$$\mathbf{G}_p(\boldsymbol{x},t) = \langle \mathbf{g}_p \rangle_p = \frac{1}{n_p(\boldsymbol{x},t)} \lim_{\mathcal{N}_f \to \infty} \frac{1}{\mathcal{N}_f} \sum_{\mathcal{N}_f} \tilde{n}_p(\boldsymbol{x},t) \langle \mathbf{g}_p(t) | \mathcal{H}_f \rangle_p = \frac{\langle \tilde{n}_p \tilde{\mathbf{g}}_p \rangle}{n_p(\boldsymbol{x},t)}, \tag{5}$$

where $n_p(\boldsymbol{x},t) =< \tilde{n}_p >$. In the following, we shall use the simplified notation

$$\langle \tilde{\mathbf{g}}_p \rangle_p = \frac{1}{n_p(\boldsymbol{x},t)} \langle \tilde{n}_p \tilde{\mathbf{g}}_p \rangle. \tag{6}$$

The above equality is consistent with Eq. (3) if $\langle \tilde{\mathbf{g}}_p \rangle_p$ represents the averaging of the Lagrangian property $\tilde{\mathbf{g}}_p(\boldsymbol{x}_p(t),t)$ which can be defined along any particle path. Lagrangian turbulent fluctuations are then defined as $\mathbf{g}'_p(t) = \mathbf{g}_p(t) - \mathbf{G}_\mathbf{p}(\boldsymbol{x}_\mathbf{p}(\mathbf{t}),\mathbf{t})$. The ensemble average may also be replaced by time or spatial average in statistically stationary or homogeneous flows respectively.

According to MEF, the instantaneous velocity of each particle is composed of two contributions, an instantaneous Eulerian velocity field and a residual velocity component

$$u_{p,i}(t) = \tilde{u}_{p,i}(\boldsymbol{x}_p(t),t) + \delta u_{p,i}(t). \tag{7}$$

The first contribution is a correlated continuous field shared by all the particles and written in an Eulerian framework, it represents the first-order moment of the conditional PDF, namely the mesoscopic particle velocity

$$\tilde{u}_{p,i}(\boldsymbol{x},t) = \langle u_{p,i}(t) | \boldsymbol{x}_p(t) = \boldsymbol{x}; \mathcal{H}_f \rangle; \tag{8}$$

the second contribution is a random spatially-uncorrelated component, associated to each particle and defined along the particle path. In the Eulerian equations, it is characterized in terms of Eulerian fields of particle velocity moments. The second-order moment of the conditional PDF is the RUM particle kinetic stress tensor $\delta R_{p,ij}(\boldsymbol{x},t) = \langle \delta u_{p,i}(t) \delta u_{p,j}(t) | \boldsymbol{x}_p(t) = \boldsymbol{x}; \mathcal{H}_f \rangle$, whose trace is twice the RUM particle kinetic energy, $2\delta\theta_p = \delta R_{p,ii}$. The third-order moment of the RUM is $\delta Q_{p,ijk}(\boldsymbol{x},t) = \langle \delta u_{p,i}(t) \delta u_{p,j}(t) \delta u_{p,k}(t) | \boldsymbol{x}_p(t) = \boldsymbol{x}; \mathcal{H}_f \rangle$. Defining the mean mesoscopic particle velocity as $U_{p,i}(\boldsymbol{x},t) = \langle \tilde{n}_p \tilde{u}_{p,i} \rangle / \langle \tilde{n}_p \rangle = \langle \tilde{u}_{p,i} \rangle_p$, the Lagrangian velocity turbulent fluctuation associated to each particle may be obtained as $u'_{p,i}(t) = u_{p,i}(t) - U_{p,i}(\boldsymbol{x}_p(t),t)$, and the partitioning written in terms of fluctuating contributions as well $u'_{p,i}(t) = \tilde{u}'_{p,i}(\boldsymbol{x}_p(t),t) + \delta u_{p,i}(t)$. Hereinafter, the contracted notation in Eq. (6) will be retained and used whenever defining macroscopic quantities from mesoscopic ones, i.e. mean mesoscopic quantities.

2.2. The local instantaneous particle Eulerian equations

In the framework of the moment approach, the transport equations of the moments of the PDF are obtained by analogy with the kinetic theory of dilute gases (Chapman and Cowling, 1939). Without gravity, in isothermal conditions and mono-dispersed regime, when the particle-to-fluid density ratio is large, only the drag force needs to be taken into account and the PDF transport equation is written as

$$\frac{\partial}{\partial t} \tilde{f}_p^{(1)} + \frac{\partial}{\partial x_j} [c_{p,j} \tilde{f}_p^{(1)}] = + \frac{\partial}{\partial c_{p,j}} \left[\frac{(c_{p,j} - u_{f@p,j})}{\tau_p} \tilde{f}_p^{(1)} \right] + \left(\frac{\partial \tilde{f}_p^{(1)}}{\partial t} \right)_{coll}. \tag{9}$$

The first term on the r.h.s. accounts for the effect of external forces acting on the particle. It is closed according to the same assumptions used for closing the Lagrangian particle equations (see, e.g. Zaichik, 1999, and the particle Lagrangian description recalled in Appendix A). The last term in Eq. (9) accounts for the modification in the distribution function due to the particle interactions (collisions, coalescence). In very dilute regimes, it may be neglected provided that the typical collision time is much greater than the particle response time. Nevertheless, the formalism may theoretically include inter-particle collisions assuming that they do not directly induce spatial correlations in the particle velocity distribution. Local and instantaneous Eulerian equations are then obtained from Eq. (9) by multiplying by any function $\gamma(\boldsymbol{u}_p)$ and integrating over the particle-velocity space. In order to account for non-linearities between fluid and particle properties, a mesoscopic particle response time is also introduced $\tilde{\tau}_p =< 1/\tau_p | \mathcal{H}_f >_p^{-1}$ where τ_p is the well known single-particle response time recalled in Appendix A. At the first order, the local and instantaneous dispersed phase is described by the evolution of the mesoscopic particle number density and velocity (Simonin et al., 2002):

$$\frac{\partial \tilde{n}_p}{\partial t} + \frac{\partial \tilde{n}_p \tilde{u}_{p,i}}{\partial x_i} = 0, \tag{10}$$

$$\frac{\partial \tilde{n}_p \tilde{u}_{p,i}}{\partial t} + \frac{\partial \tilde{n}_p \tilde{u}_{p,i} \tilde{u}_{p,j}}{\partial x_j} = -\frac{\tilde{n}_p}{\tilde{\tau}_p} (\tilde{u}_{p,i} - u_{f,i}) - \frac{\partial \tilde{n}_p \delta R_{p,ij}}{\partial x_j}. \tag{11}$$

In Eq. (11), the first term on the r.h.s. accounts for the effects of the drag force and the second term is the transport due to RUM. At the second order, the statistical modeling leads to an equation for the RUM particle kinetic stress tensor (Moreau, 2006):

$$\frac{\partial \tilde{n}_p \delta R_{p,ij}}{\partial t} + \frac{\partial \tilde{n}_p \delta R_{p,ij} \tilde{u}_{p,k}}{\partial x_k} = -2 \frac{\tilde{n}_p}{\tilde{\tau}_p} \delta R_{p,ij} - \tilde{n}_p \delta R_{p,jk} \frac{\partial \tilde{u}_{p,i}}{\partial x_k} - \tilde{n}_p \delta R_{p,ik} \frac{\partial \tilde{u}_{p,j}}{\partial x_k} - \frac{\partial}{\partial x_k} \tilde{n}_p \delta Q_{p,ijk}. \tag{12}$$

In Eq. (12), the first term on the r.h.s. is the dissipation of the RUM stresses by the fluid drag. Second and third terms represent the production of RUM by mesoscopic velocity gradients; however, they may have local negative sign corresponding to an inverse energy exchange. The last term in Eq. (12) is the contribution to the transport by the third-order RUM correlation. System (10)–(12), represents an unclosed set of equations which requires the modeling of the third-order velocity moment in order to be used for predicting the local and instantaneous dispersed phase. As an alternative, the first order modeling (i.e. Eqs. (10) and (11)) may be used, provided that a closure for the RUM stress tensor is given. In this work, a first-order ACBMM is developed. Its success depends on the accuracy of the RUM algebraic closure.

3. The RUM particle kinetic stress tensor

The goal of this study is to provide a constitutive relation which makes it possible to write the RUM tensor as a function of known quantities. A quantity that seems to be appropriate for this purpose is the particle rate-of-strain tensor. In this section the two tensors are described and some important results of a previous analysis carried out on the structure of the tensors briefly exposed (further details may be found in Masi et al. (2010)).

3.1. Analogy with the kinetic theory and RANS algebraic closures

The RUM tensor, $\delta R_{p,ij}$, may be considered as the equivalent of the stress tensor in the Navier–Stokes (NS) equations, similarly derived by using the Boltzmann kinetic theory. It consists of an isotropic and a deviatoric parts:

$$\delta R_{p,ij} = \frac{1}{3} \delta R_{p,kk} \delta_{ij} + \delta R^*_{p,ij} = \frac{2}{3} \delta\theta_p \delta_{ij} + \delta R^*_{p,ij}. \tag{13}$$

By analogy with fluids, the isotropic part may be assimilated to a mechanical pressure and the deviatoric part to a viscous contribution. The isotropic part, involving the RUM kinetic energy $\delta\theta_p$,

may be obtained by an additional transport equation (Simonin et al., 2002)

$$\frac{\partial \tilde{n}_p \delta\theta_p}{\partial t} + \frac{\partial \tilde{n}_p \delta\theta_p \tilde{u}_{p,m}}{\partial x_m} = -\tilde{n}_p \delta R_{p,nm} \frac{\partial \tilde{u}_{p,n}}{\partial x_m} - 2\frac{\tilde{n}_p}{\tilde{\tau}_p}\delta\theta_p - \frac{1}{2}\frac{\partial}{\partial x_m}\tilde{n}_p \delta Q_{p,nnm} \quad (14)$$

and only the deviatoric part needs to be modeled (in addition with the contracted triple velocity correlation $\delta Q_{p,nnm}$ for which closures are given elsewhere (Moreau, 2006; Kaufmann et al., 2008)).

In order to close the stress tensor in the NS equations, the well-known hypotheses leading to formulate the constitutive relations for Stokesian and Newtonian fluids are formulated. To the general principles of determinism, indifference from the reference frame and local effect, a linear relationship between the stresses and the rate-of-strain tensor, for Newtonian fluids, is assumed. It may be supposed that the behavior of the dispersed phase (modeled as a continuum) is instead far from that of Newtonian fluids. If time-history and non-local effects could be disregarded as a first approximation, a linear relationship between the RUM and the particle rate-of-strain tensors seems instead inadequate. For the NS stress tensor, Chen et al. (2004) provided an analytical expression using a Chapman–Enskog expansion applied to the Boltzmann equation. They showed that the first-order approximation leads to the well-known constitutive relation for Newtonian fluids, while the second-order approximation leads to a "non-Newtonian" expression in which the stresses are related to a "memory-effect" term, represented by the Lagrangian derivative of the strain, and to non-linear tensorial terms. Assuming analogy between thermal fluctuations and turbulent fluctuations of the fluid (DNS versus RANS tensor), Chen et al. (2004) provided an expression for the Reynolds stresses accounting for the second-order approximation in the Chapman–Enskog expansion. It is noteworthy that this expression turned out very similar to the second-order turbulence models, encouraging the analogy between turbulent eddies and thermal fluctuations. Using a similar analogy for the dispersed phase, but in reverse (RANS versus DNS), linear and non-linear constitutive relations for the RUM tensor may be provided by means of algebraic closures which are derived by analogy with first-order and second-order approximation models in turbulence. However, the reader is cautioned against confusing the RUM particle kinetic stress tensor, which is local and instantaneous, with a Reynolds-like stress tensor, which is not. In this work, the non-linearity aspect of the constitutive relation will be emphasized.

3.2. RUM, anisotropy, and particle rate-of-strain tensors

The particle rate-of-strain tensor, $S_{p,ij}$, represents the symmetric part of the mesoscopic particle velocity-gradient tensor which is defined as follows:

$$\frac{\partial \tilde{u}_{p,i}}{\partial x_j} = \frac{1}{2}\left(\frac{\partial \tilde{u}_{p,i}}{\partial x_j} + \frac{\partial \tilde{u}_{p,j}}{\partial x_i}\right) + \frac{1}{2}\left(\frac{\partial \tilde{u}_{p,i}}{\partial x_j} - \frac{\partial \tilde{u}_{p,j}}{\partial x_i}\right) = \left(S^*_{p,ij} + \frac{1}{3}S_{p,kk}\delta_{ij}\right) + \Omega_{p,ij}; \quad (15)$$

the deviatoric part of the strain, $S^*_{p,ij}$, accounts for shearing or distortion of any element of the dispersed phase while the isotropic part, $\frac{1}{3}S_{p,kk}\delta_{ij}$, accounts for contraction or expansion. The angular rotation of any element of the dispersed phase is then represented by the antisymmetric contribution of the particle velocity-gradient tensor, namely the mesoscopic particle vorticity tensor, $\Omega_{p,ij}$. Hereinafter, matrix notation will be frequently used. When associated with a tensor, bold notation denotes three-dimensional second-order tensors, curly brackets $\{\cdot\}$ represent the trace, and the asterisk means traceless tensor. The inner product of two second-order tensors is then defined in a matrix notation as $\mathbf{C} = \mathbf{AB} = A_{ik}B_{kj} = C_{ij}$, $\mathbf{B^2} = \mathbf{BB}$ and $\mathbf{I}$ is the identity matrix.

In order to study the structure of the deviatoric RUM, $\mathbf{R}^*$, and the particle rate-of-strain, $\mathbf{S}^*$, tensors the authors (Masi et al., 2010) used a local dimensionless parameter, s^*, originally proposed by Lund and Rogers (1994) and employed by several authors involved in one-phase turbulent flow analyses (see, e.g. Tao et al., 2002; Higgins et al., 2003). This parameter, originally called "strain-state parameter" and used to study the "shape" of the deformation caused by the fluid rate-of-strain tensor, may be used to investigate the structure of any traceless real and symmetric tensor giving local information about the relative magnitude of the tensor eigenvalues, reproducing information similar to that provided by the invariant Lumley's map (Lumley, 1978) but for local and instantaneous (not averaged) tensors. An important finding of the authors's analysis was to show that in very dilute regime the tensors $\mathbf{R}^*$ and $\mathbf{S}^*$ behave, in principal axes, as in a state of axisymmetric contraction and expansion respectively, regardless of the particle inertia. The state of axisymmetric expansion of $\mathbf{S}^*$ (particle strain) was found to be the most probable among all the possible states of the tensor during the simulation. It is comparable to the state of axisymmetric expansion of the fluid rate-of-strain tensor (turbulent local and instantaneous strain); the latter observation is consistent with the study of Lund and Rogers (1994) who found the expansion the most probable state of the fluid strain in HIT. But most important, the authors showed that, in very dilute regime, the RUM tensor behaves as in a one-component state which represents the limit case of an axisymmetric contraction (based on the shape of the RUM tensor, implying that the smallest eigenvalues of RUM tend to zero). From a physical point of view, this means that the RUM agitation develops in one preferred (local and instantaneous) direction while it is damped in the others. In turbulent fluid flows, the one-component limit is the long-time asymptotic solution provided by the rapid distortion theory (Rogers, 1991) of a HIT submitted to a strong shear. Then, a redistribution of energy between the stresses is ensured by the action of the pressure-strain correlations. The authors conjectured that in very dilute regimes, where inter-particle collisions are negligible, the dispersed phase submitted to a strong shear develops anisotropy which achieves and preserves the theoretical asymptotic values of the one-component limit, as no redistribution between stresses is possible neglecting collisions. In contrast, accounting for collisions should introduce a new term in the RUM stress transport equation which accounts for a redistribution effect. In the frame of the Grad's theory, this term may be modeled (Simonin, 1991b) similarly to the return-to-isotropy Rotta's model developed for pressure-strain correlation in turbulent flows (Rotta, 1951). For larger values of the solid volume fraction, the dispersed phase should move away from the one-component limit state as the collision frequency increases. This effect of redistribution by collisions has been clearly shown by Vance et al. (2006) in their numerical simulations of a fully developed particle-laden turbulent channel flow. From a modeling point of view, the one-component limit state is very helpful as, in this case, the eigenvalues of anisotropy are known with the consequence that also its invariants are. Indeed, according to Lumley (1978), the eigenvalues of the (generic) anisotropy tensor $\mathbf{g}^* = \frac{\mathbf{G}}{\{\mathbf{G}\}} - \frac{1}{3}\mathbf{I} = \frac{\mathbf{G}^*}{\{\mathbf{G}\}}$ corresponding to the one-component limit state are $\lambda_1 = \frac{2}{3}$, $\lambda_2 = \lambda_3 = -\frac{1}{3}$. The same applies for the local and instantaneous RUM particle anisotropy tensor which is defined as follows:

$$b^*_{p,ij} = \frac{\delta R_{p,ij}}{2\delta\theta_p} - \frac{1}{3}\delta_{ij}. \quad (16)$$

These information will be used for building some of the constitutive relations proposed in Section 4 and for an analysis purpose.

4. Modeling the deviatoric RUM particle kinetic stress tensor

This section is devoted to the modeling of the deviatoric RUM particle kinetic stress tensor. A brief description of existing algebraic closures is given and new algebraic closures are developed.

4.1. Local equilibrium assumption of the stresses

In order to close the deviatoric RUM tensor, an equilibrium hypothesis over the tensor components is first retained. The equation for $\delta R^*_{p,ij}$ may be obtained by subtracting Eq. (14) (multiplied by $\frac{2}{3}\delta_{ij}$) from Eq. (12). The equilibrium assumption then entails neglecting transport terms and equation reduces to the form

$$\delta R^*_{p,ij} = -\frac{\tilde{\tau}_p}{2}\left[\frac{2}{3}\delta\theta_p\left(\frac{\partial \tilde{u}_{p,i}}{\partial x_j}+\frac{\partial \tilde{u}_{p,j}}{\partial x_i}-\frac{2}{3}\frac{\partial \tilde{u}_{p,m}}{\partial x_m}\delta_{ij}\right)\right] - \frac{\tilde{\tau}_p}{2}\left[\delta R^*_{p,jk}\frac{\partial \tilde{u}_{p,i}}{\partial x_k}+\delta R^*_{p,ik}\frac{\partial \tilde{u}_{p,j}}{\partial x_k}-\frac{2}{3}\delta R^*_{p,mn}\frac{\partial \tilde{u}_{p,m}}{\partial x_n}\delta_{ij}\right]. \quad (17)$$

This expression may be further simplified assuming light anisotropy; in this case the second-order approximation in Eq. (17) may be neglected and the expression turns into the well known viscosity-like model proposed, for the dispersed phase, by Simonin et al. (2002). It may be reformulated in terms of a RUM viscosity as

$$\delta R^*_{p,ij} = -2\nu_t S^*_{p,ij}, \quad (18)$$

where $\nu_t = \tilde{\tau}_p\delta\theta_p/3$. Hereinafter, Eq. (18) will be referred to as VISCO model.

4.2. Viscosity-like model from axisymmetric tensors

The model presented in this section is based on the work of Jovanović and Otić (2000) originally proposed for turbulent flows. According to numerical observations (Masi et al., 2010) tensors are assumed axisymmetric with respect to a (same) direction and written in a bilinear form (Batchelor, 1946; Chandrasekhar, 1950) as

$$S^*_{p,ij} = A\delta_{ij} - 3A\lambda_i\lambda_j, \quad (19)$$

$$\delta R^*_{p,ij} = C\delta_{ij} - 3C\lambda_i\lambda_j. \quad (20)$$

Defining the magnitude of the particle rate-of-strain tensor as $S = II_S^{1/2}$, where $II_S = \{\mathbf{S}^{*2}\}$ is the second dimensional invariant of the tensor, the quantity A may be expressed as a function of S and used to re-formulate Eq. (19) as a function of the unique unknown quantity $\lambda_i\lambda_j$. The latter is then explicitly obtained and injected into Eq. (20) from which the deviatoric RUM stress tensor is obtained, provided that the magnitude of the anisotropy tensor is known (i.e. its second invariant). Further manipulations (detailed in Masi et al. (2010)) lead to the expression

$$\delta R^*_{p,ij} = sign(III_S)\left(\frac{2}{3}\right)^{1/2} 2\delta\theta_p\frac{S^*_{p,ij}}{S}, \quad (21)$$

where $III_S = \{\mathbf{S}^{*3}\}$ is the third (dimensional) invariant of the particle rate-of-strain tensor. In the above model, the axisymmetry of the tensors, their alignment, and the one-component limit state of stresses are assumed. Under such assumptions, the sign of III_S reproduces both positive and negative viscosities corresponding to an axisymmetric particle rate-of-strain tensor which moves from a configuration of expansion to contraction and vice versa. Contracting Eq. (21) by multiplying by the tensor $S^*_{p,ij}$ gives an expression for the scalar quantity $\delta R^*_{p,ij}S^*_{p,ij}$ which represents the production of the RUM kinetic energy by shear (corresponding to the deviatoric-RUM contribution of the first r.h.s. term in Eq. (14)) multiplied by $-1/\tilde{n}_p$. This makes it possible to write $\delta R^*_{p,ij}S^*_{p,ij}$ as a function of the second invariant of the particle rate-of-strain tensor, the RUM kinetic energy, both positive quantities, and the sign of III_S. The correlation between the sign of III_S and that of $\delta R^*_{p,ij}S^*_{p,ij}$ will be investigated in Section 6. Hereinafter, the model (21) will be referred to as AXISY-C. For a comparison purpose, it will be also tested accounting for only a positive viscosity (negative sign into the model which represents the most probable sign), and the model referred to as AXISY.

4.3. Quadratic algebraic approximation

Assuming equilibrium of the components of the RUM stress tensor, as in Section 4.1, Zaichik (2009) suggested a model which, from Eq. (17), applies an iteration procedure invoking the isotropic approximation at the zero-order iteration (i.e. $\delta R^{*(0)}_{p,ij} = 0$), assuming that $\epsilon = \tilde{\tau}_p S$ is a small parameter. The first-order approximation is equivalent to the model suggested by Simonin et al. (2002) and recalled in Section 4.1, namely the model VISCO. The second-order approximation is obtained from Eq. (17) using the first-order approximation (18), leading to

$$\delta R^*_{p,ij} = -\frac{2\tilde{\tau}_p\delta\theta_p}{3}S^*_{p,ij} + \frac{2\tilde{\tau}_p^2\delta\theta_p}{6}\left(S^*_{p,ik}\frac{\partial \tilde{u}_{p,j}}{\partial x_k}+S^*_{p,jk}\frac{\partial \tilde{u}_{p,i}}{\partial x_k}-\frac{2}{3}S^*_{p,mn}\frac{\partial \tilde{u}_{p,m}}{\partial x_n}\delta_{ij}\right). \quad (22)$$

According to Zaichik (2009), Eq. (22) agrees with the second-order approximation obtained by solving the BGK form Bhatnagar et al. (1954) of the Boltzmann kinetic equation by means of a Chapman–Enskog expansion technique (Chapman and Cowling, 1939). Chen et al. (2004) used such an expansion to obtain deviations from equilibrium at various orders of the Knudsen number ($\mathcal{K}$). The latter was defined as the ratio between the turbulent time and a representative timescale of the mean field, and used as a small parameter in their perturbation expansion of the turbulent Boltzmann equation (similarly to the parameter ϵ of the Zaichik's model). The small parameter legitimates the use of a perturbation expansion around a state of equilibrium and defines the accuracy of the truncated approximate solution. In the model of Chen et al. (2004), developed to provide high-order terms for the Reynolds stress tensor, the BGK equation is expanded neglecting only the terms due to the finite compressibility. In their second-order approximation, a term accounting for the Lagrangian time derivative of the rate-of-strain tensor appears, unlike the Zaichik's model. The difference is due to the fact that in the Zaichik's model the iteration procedure is applied to an equilibrium expression devoid of transport terms as a starting point, while in Chen et al. (2004) the differential operators included in the original transport equation are also expanded. The Lagrangian time derivative of the rate-of-strain tensor would make appear additional terms in the constitutive relation. This point will not be addressed in the frame of a quadratic algebraic approximation. Instead, an improved model which does not rely on neglecting transport terms in the stress transport equations and which contains additional tensors is developed by the next section. Hereinafter, Eq. (22) will be referred to as QUAD model.

4.4. Self-similarity assumption: 2ΦEASM models

Inspired from the well-known model suggested by Rodi (1972) for closing the Reynolds stress tensor in turbulence, an equilibrium assumption over the components of the RUM anisotropy is proposed. This model relies on the assumption that the RUM stress tensor is a self-similar tensor which means that its temporal and spatial variations are related to that of its trace. The self-similarity assumption leads to write

$$\frac{D}{Dt}b^*_{p,ij} = 0 \quad \text{with} \quad \frac{D}{Dt} = \frac{\partial}{\partial t}+\tilde{u}_{p,k}\frac{\partial}{\partial x_k}. \quad (23)$$

Using definition (16), the above relation is re-written as follows

$$\frac{D}{Dt}\delta R_{p,ij} = \frac{\delta R_{p,ij}}{\delta\theta_p}\frac{D}{Dt}\delta\theta_p. \tag{24}$$

Then, injecting Eqs. (12) and (14) into Eq. (24) yields

$$\delta R_{p,jk}\frac{\partial\tilde{u}_{p,i}}{\partial x_k} + \delta R_{p,ik}\frac{\partial\tilde{u}_{p,j}}{\partial x_k} + \frac{2}{\tilde{\tau}_p}\delta R_{p,ij} + \frac{1}{\tilde{n}_p}\frac{\partial}{\partial x_k}\tilde{n}_p\delta Q_{p,ijk} = \frac{\delta R_{p,ij}}{\delta\theta_p}\left[\delta R_{p,nm}\frac{\partial\tilde{u}_{p,n}}{\partial x_m} + \frac{2}{\tilde{\tau}_p}\delta\theta_p + \frac{1}{2}\frac{1}{\tilde{n}_p}\frac{\partial}{\partial x_m}\tilde{n}_p\delta Q_{p,nnm}\right]. \tag{25}$$

Finally, assuming equality between third-order correlations and rearranging some terms, the equation takes the form

$$\delta R_{p,ij}\left(-\frac{\delta R_{p,nm}}{2\delta\theta_p}\frac{\partial\tilde{u}_{p,n}}{\partial x_m}\right) = -\frac{1}{2}\delta R_{p,jk}\frac{\partial\tilde{u}_{p,i}}{\partial x_k} - \frac{1}{2}\delta R_{p,ik}\frac{\partial\tilde{u}_{p,j}}{\partial x_k}. \tag{26}$$

The term within the parentheses represents the normalized (by $2\delta\theta_p$) production of the RUM kinetic energy by shear and compression, which may be written as $-\{\mathbf{b}^*\mathbf{S}^*\} - \frac{1}{3}\{\mathbf{S}\}$. Before tackling the problem of the solution of the system (26), the system is re-written in terms of anisotropy and particle rate-of-strain and vorticity tensors, by using definitions (15) and (16). Dividing Eq. (26) by $2\delta\theta_p$, subtracting the trace from both the l.h.s. and r.h.s. tensors and accounting for compressibility (the trace of $\mathbf{S}$ is not null), the equation takes the form

$$\mathbf{b}^*(-2\{\mathbf{b}^*\mathbf{S}^*\}) = -\frac{2}{3}\mathbf{S}^* - (\mathbf{b}^*\mathbf{S}^* + \mathbf{S}^*\mathbf{b}^* - \frac{2}{3}\{\mathbf{b}^*\mathbf{S}^*\}\mathbf{I}) + (\mathbf{b}^*\boldsymbol{\Omega} - \boldsymbol{\Omega}\mathbf{b}^*). \tag{27}$$

The system (27) is nonlinear and implicit since the production term (on the l.h.s.) also involves the anisotropy tensor, and because the system is expressed in terms of $\mathbf{b}^*$, as well as of $\mathbf{S}^*$ and $\boldsymbol{\Omega}$. Eq. (27) is a novel implicit 2ΦASM closure for the RUM stress tensor. Hereinafter, all the models arisen from an explicit solution of this set of linearized equations will be referred to as 2ΦEASM models. It is worth of note that a hypothesis of self-similarity of the RUM stress tensor leads to an Eq. (26) devoid of drag dissipation terms. Indeed, as the dissipations in Eqs. (12) and (14) are linear terms, under a self-similarity hypothesis their contribution disappear. For this reason, the particle response time is no longer accounted for into the model. This result is extremely important as it shows that an assumption of equilibrium of anisotropy does not rely directly on the particle inertia. This finding will reveal a focal point of the modeling.

4.4.1. The problem of the explicit algebraic solution

Since a numerical solution of the implicit 2ΦASM closure (27) is not straightforward and may be computationally expensive, an explicit solution is sought. In this section we describe the explicit solution of the system assuming to be linear, tackling in a second time the problem of the linearization. Eq. (27) is rewritten as follows:

$$\mathbf{b}^+ = -\mathbf{S}^+ - \left(\mathbf{b}^+\mathbf{S}^+ + \mathbf{S}^+\mathbf{b}^+ - \frac{2}{3}\{\mathbf{b}^+\mathbf{S}^+\}\mathbf{I}\right) + (\mathbf{b}^+\boldsymbol{\Omega}^+ - \boldsymbol{\Omega}^+\mathbf{b}^+) \tag{28}$$

where $\mathbf{b}^+ = \frac{3}{2}\mathbf{b}^*$, and $\mathbf{S}^+ = \mathbf{S}^*/(-2\{\mathbf{b}^*\mathbf{S}^*\})$ and $\boldsymbol{\Omega}^+ = \boldsymbol{\Omega}/(-2\{\mathbf{b}^*\mathbf{S}^*\})$ are the normalized traceless particle rate-of-strain and vorticity tensors, respectively. According to Pope (1975), the anisotropy can be expressed by the form

$$\mathbf{b}^+ = \sum_\varsigma G_\varsigma \mathbf{T}_\varsigma \tag{29}$$

which represents the linear combination of a set of non-dimensional independent, symmetric and deviatoric second-order tensors $\mathbf{T}_\varsigma$, using scalar coefficients G_ς which are functions of the invariants of $\mathbf{S}^+$ and $\boldsymbol{\Omega}^+$. Using the Cayley–Hamilton theorem, Pope (1975) showed that a set of ten ($\varsigma = 10$) tensors $\mathbf{T}_\varsigma$ needs to form an integrity basis Spencer (1971) in order to express every symmetric deviatoric second-order tensor formed by $\mathbf{S}^+$ and $\boldsymbol{\Omega}^+$. The ten tensors are recalled in Table 1. Concerning coefficients G_ς, Gatski and Speziale (1993) gave the general solution for fully three-dimensional flows involving ten coefficients. They are functions of the five invariants

$$\eta_1 = \{\mathbf{S}^{+2}\}, \quad \eta_2 = \{\boldsymbol{\Omega}^{+2}\}, \quad \eta_3 = \{\mathbf{S}^{+3}\}, \quad \eta_4 = \{\mathbf{S}^+\boldsymbol{\Omega}^{+2}\}, \quad \eta_5 = \{\mathbf{S}^{+2}\boldsymbol{\Omega}^{+2}\}. \tag{30}$$

According to Eq. (29), the resulting solution is fully explicit and its implementation straightforward. The use of the complete ten-tensor basis is referred to as 3D form of the model. As an alternative, a two-dimensional approximation using only a three-tensor basis may also apply for three-dimensional flows. Two-dimensional flows are mean-quantity free in one of the three directions. According to Gatski and Speziale (1993), in that case only three tensors are needed as integrity basis, which are $\mathbf{T}_1$, $\mathbf{T}_2$, $\mathbf{T}_3$. Moreover under the two-dimensional assumption the invariants η_3 and η_4 are zero and η_5 is equal to $\frac{1}{2}\eta_1\eta_2$. The resulting 2D expression is

$$\mathbf{b}^+ = -\frac{3}{3 - 2\eta_1 - 6\eta_2}\left[\mathbf{S}^+ + (\mathbf{S}^+\boldsymbol{\Omega}^+ - \boldsymbol{\Omega}^+\mathbf{S}^+) - 2\left(\mathbf{S}^{+2} - \frac{1}{3}\{\mathbf{S}^{+2}\}\mathbf{I}\right)\right]. \tag{31}$$

Eq. (31) is easier to handle than Eq. (29) when the denominator vanishes and singularities appear (details may be found in Gatski and Speziale (1993)). A regularization procedure is indeed available for the 2D form (Gatski and Speziale, 1993) while, to the best of our knowledge, no regularization procedure exists for the fully three-dimensional solution because of its cumbersome form. In our case, because of the assumptions detailed in Section 4.4.2, no regularization procedure is necessary.

In the literature of turbulent fluid flows, explicit solutions of an equilibrium anisotropy assumption are often referred to as EASM (as explicit algebraic stress models) or EARSM (as explicit algebraic Reynolds stress models). In the past decades, several studies on the theoretical and numerical aspects of these models have been carried out; an overview may be gained from the works of Pope (1975), Rodi (1976), Taulbee (1992), Speziale and Xu (1996), Girimaji (1997a), Wallin and Johansson (2002), Weis and Hutter (2003), Gatski and Wallin (2004), Grundestam et al. (2005) in which many different aspects of the modeling have been addressed as, for example, non-equilibrium flows, invariance from the frame of reference, numerical methods. This bibliography is clearly not exhaustive, but it is enough to understand the multitude of questions arisen from the EASM approaches. Concerning an analogous formulation for modeling the local deviatoric RUM particle kinetic stress tensor in the framework of an Eulerian approach for the dispersed phase, no literature exists. This is why we stay on the simpler original idea on which the approach is based, leaving as a perspective the handling of more sophisticate aspects of such models.

Table 1
The integrity basis for fully three-dimensional flows.

$\mathbf{T}_1 = \mathbf{S}^+$	$\mathbf{T}_6 = \boldsymbol{\Omega}^{+2}\mathbf{S}^+ + \mathbf{S}^+\boldsymbol{\Omega}^{+2} - \frac{2}{3}\{\mathbf{S}^+\boldsymbol{\Omega}^{+2}\}\mathbf{I}$
$\mathbf{T}_2 = \mathbf{S}^+\boldsymbol{\Omega}^+ - \boldsymbol{\Omega}^+\mathbf{S}^+$	$\mathbf{T}_7 = \boldsymbol{\Omega}^+\mathbf{S}^+\boldsymbol{\Omega}^{+2} - \boldsymbol{\Omega}^{+2}\mathbf{S}^+\boldsymbol{\Omega}^+$
$\mathbf{T}_3 = \mathbf{S}^{+2} - \frac{1}{3}\{\mathbf{S}^{+2}\}\mathbf{I}$	$\mathbf{T}_8 = \mathbf{S}^+\boldsymbol{\Omega}^+\mathbf{S}^{+2} - \mathbf{S}^{+2}\boldsymbol{\Omega}^+\mathbf{S}^+$
$\mathbf{T}_4 = \boldsymbol{\Omega}^{+2} - \frac{1}{3}\{\boldsymbol{\Omega}^{+2}\}\mathbf{I}$	$\mathbf{T}_9 = \boldsymbol{\Omega}^{+2}\mathbf{S}^{+2} + \mathbf{S}^{+2}\boldsymbol{\Omega}^{+2} - \frac{2}{3}\{\mathbf{S}^{+2}\boldsymbol{\Omega}^{+2}\}\mathbf{I}$
$\mathbf{T}_5 = \boldsymbol{\Omega}^+\mathbf{S}^{+2} - \mathbf{S}^{+2}\boldsymbol{\Omega}^+$	$\mathbf{T}_{10} = \boldsymbol{\Omega}^+\mathbf{S}^{+2}\boldsymbol{\Omega}^{+2} - \boldsymbol{\Omega}^{+2}\mathbf{S}^{+2}\boldsymbol{\Omega}^+$

4.4.2. Modeling the non-linearity

Unfortunately, the explicit solution procedure described in Section 4.4.1 does not address the concern of the system linearization. Indeed, Gatski and Speziale (1993) needed to add further assumptions to express their analogous term P/ϵ, evoking equilibrium for homogeneous turbulent flows which leads to set P/ϵ as a constant. Similarly, in order to use this method, we need an expression for the term $-2\{\mathbf{b}^*\mathbf{S}^*\}$. As recalled in Section 3, a previous analysis about the structure of the tensors showed that $\mathbf{R}^*$ and $\mathbf{S}^*$ are both axisymmetric, behaving as in a one-component limit and as in axisymmetric expansion (as most probable state), respectively. In this case, the eigenvalues of RUM anisotropy are $\lambda_1 = \frac{2}{3}$, $\lambda_2 = \lambda_3 = -\frac{1}{3}$ and that of the rate-of-strain tensor are $\lambda_1 = -2S_\lambda$, $\lambda_2 = \lambda_3 = S_\lambda$ where S_λ is the largest eigenvalue of $\mathbf{S}^*$. Then assuming alignment between tensors and between axisymmetric directions, the contracted product $b^*_{p,ij}S^*_{p,ij}$ may be written in principal axes as $b^*_{p,ij}S^*_{p,ij} = -2S_\lambda$. Similarly, we write the contracted product $S^*_{p,ij}S^*_{p,ij} = 6S^2_\lambda = II_S$. Relating these two expressions we finally obtain

$$-2\{\mathbf{b}^*\mathbf{S}^*\} = 2\left(\frac{2}{3}\right)^{1/2} II_S^{1/2}. \tag{32}$$

This term is invariant by definition, hence it may be used in any coordinate system. Injecting Eq. (32) into the fully 3D form (29) or into the 2D form of the model (31), the system is then linearized and a solution may be explicitly obtained. While there is no mathematical guarantee that singularities do not occur in the 3D solution, we can demonstrate that in our case, in which tensors are normalized using Eq. (32), the 2D form is always nonsingular. Indeed, writing the denominator $D = 3 - 2\eta^2 + 6\zeta^2$ using the quantities $\eta = \sqrt{\eta_1}$ and $\zeta = \sqrt{-\eta_2}$ which explicitly account for the sign of the invariants, in the limit case in which ζ^2 is zero, otherwise it is always greater than zero because positive, it should be $\eta^2 < 1.5$ in order to avoid that D vanishes. Computing $\eta^2 = \eta_1$ from the normalized tensor $\mathbf{S}^+$, it is clear that this condition is always accomplished. Therefore, stable solutions may always be obtained using the linearized explicit 2D-form of the system, Eq. (31), in conjunction with approximation (32). In this study, only the 2D-model predictions will be presented and referred to as 2ΦEASM1 model. Indeed, results from the 3D form of the model have shown that no improvement is obtained when the full-tensor basis is used in conjunction with the approximation (32). The 3D form is therefore discarded.

4.4.3. An explicit solution accounting for the non-linearity

In the literature of turbulent fluid flows, fully-explicit and self-consistent solutions directly accounting for the nonlinearity were suggested, for example, by Girimaji (1996) and Wallin and Johansson (2000). In the framework of the two-dimensional approximation, these two techniques lead to the same solution. However, the technique of Wallin and Johansson (2000) additionally provides a three-dimensional form of the model and it is thus retained in this study. Originally conceived for the turbulence equations, it is here applied to our 2ΦASM model (27). In order to facilitate the reading, we will use the same notation as in Wallin and Johansson (2000). According to the Wallin & Johansson's notation, the dispersed-phase anisotropy equation is written as

$$N\mathbf{b}^* = -A_1\mathbf{S}^+ - A_2\left(\mathbf{b}^*\mathbf{S}^+ + \mathbf{S}^+\mathbf{b}^* - \frac{2}{3}\{\mathbf{b}^*\mathbf{S}^+\}\mathbf{I}\right) + (\mathbf{b}^*\mathbf{\Omega}^+ - \mathbf{\Omega}^+\mathbf{b}^*) \tag{33}$$

where N, by analogy with Wallin and Johansson (2000), is defined as $N = A_3 + A_4\,(-\{\mathbf{b}^*\mathbf{S}^+\})$, and $\mathbf{S}^+$ and $\mathbf{\Omega}^+$ are the dimensionless (by the quantity $II_S^{1/2}$, for example) particle rate-of-strain and vorticity tensors (note that dimensional tensors may also be used; in that case dimensional invariants have to be employed). Comparing the systems (27) and (33), the coefficients take the values $A_1 = \frac{2}{3}$, $A_2 = 1$, $A_3 = 0$, $A_4 = 2$. The Wallin and Johansson's technique consists in injecting the general form of the anisotropy (29) (in which $\mathbf{b}^+ = \mathbf{b}^*$) into Eq. (33). This leads to formulate the ten coefficients as a function of N and the latter becomes the only unknown term which needs to be solved. The ten scalar coefficients are functions of the five invariants (30). For fully three-dimensional flows, the solution gives a sixth-order polynomial in N, which is complex to handle. Alternatively, a two-dimensional solution, consisting in a third-order polynomial in N, may be retained and used in both the 2D and 3D forms of the model. The latter may be considered as an approximate 3D solution and it will be referred to as 3D-A. In very dilute regime in which A_3 is zero, the third-order polynomial is depressed to a pure quadratic equation as follows

$$N^2 = \left[\left(A_1A_4 + \frac{2}{3}A_2^2\right)\eta_1 + 2\eta_2\right] = 2\eta_1 + 2\eta_2. \tag{34}$$

For fully-three dimensional flows the ten coefficients provided by Wallin and Johansson (2000) are recalled in Table 2 where Q is

$$\begin{aligned} Q = {} & +3N^5 + \left(-\frac{15}{2}\eta_2 - \frac{7}{2}A_2^2\eta_1\right)N^3 + (21A_2\eta_4 - A_2^3\eta_3)N^2 \\ & + \left(3\eta_2^2 - 8\eta_1\eta_2A_2^2 + 24A_2^2\eta_5 + A_2^4\eta_1^2\right)N + \frac{2}{3}A_2^5\eta_1\eta_3 \\ & + 2A_2^3\eta_4\eta_1 - 2A_2^3\eta_2\eta_3 - 6\eta_4A_2\eta_2. \end{aligned} \tag{35}$$

Instead, according to the two-dimensional approximation the coefficients become

$$\begin{aligned} & G_1 = -\frac{A_1N}{Q}, \quad G_2 = -\frac{A_1}{Q}, \quad G_3 = 2\frac{A_1A_2}{Q}, \quad G_i = 0, \\ & i \in [4, 10]; \quad \text{with} \quad Q = N^2 - 2\eta_2 - \frac{2}{3}A_2^2\eta_1. \end{aligned} \tag{36}$$

For both the 2D and 3D forms, an explicit solution for the anisotropy tensor is finally obtained inserting coefficients (36) and Table 2, respectively, into the tensor polynomial expression (29), using the integrity basis in Table 1. However, only the 2D form of the model ensures nonsingular solutions. Indeed, injecting Eq.(34) into the definition of the denominator (36), it is clear that Q never vanishes if $\eta_1 \neq 0$. Examinations of Eq.(34) leads to conclude that as η_2 is always negative, the polynomial admits real solutions only for $\eta^2 \geqslant \zeta^2$. In order to use this model, local negative values of the discriminant will be set to zero. The legitimacy of such an approximation will be checked in Section 6. Alternatively, one could assume dilute rather than very dilute regime. The latter implies that the inter-particle collision time is much larger than the particle relaxation time, so that collisions may be neglected. If the two timescales are instead of the same order of magnitude and the volume-fraction rate is small ($\alpha_p \leqslant 0.01$), the regime can still be considered as dilute, i.e.no modulation of the turbulence by the presence of the particles occurs, but collisions should be taken into account. In this case the model coefficient A_3 is no longer zero, as it accounts for the effects of collisions on the anisotropy, and N is found as the solution of a third-order polynomial. This concern is not addressed by the present study as we assumed very dilute regime. Concerning the sign of

Table 2
Coefficients associated to the integrity basis.

$G_1 = -\frac{1}{2}A_1N\left(30A_2\eta_4 - 21N\eta_2 - 2A_2^3\eta_3 + 6N^3 - 3A_2^2\eta_1N\right)/Q$	$G_6 = -9A_1N^2/Q$
$G_2 = -A_1\left(2A_2^3\eta_3 + 3A_2^2N\eta_1 + 6A_2\eta_4 - 6N\eta_2 + 3N^3\right)/Q$	$G_7 = 9A_1N/Q$
$G_3 = -A_1A_2\left(6A_2\eta_4 + 12N\eta_2 + 2A_2^3\eta_3 - 6N^3 + 3A_2^2\eta_1N\right)/Q$	$G_8 = 9A_1A_2^2N/Q$
$G_4 = -3A_1\left(2A_2^2\eta_3 + 3NA_2\eta_1 + 6\eta_4\right)/Q$	$G_9 = 18A_1\,A_2N/Q$
$G_5 = -9A_1A_2N^2/Q$	$G_{10} = 0$

N, the following considerations are done. According to the two-dimensional approximation, the general representation of the three-dimensional anisotropy tensor is $\mathbf{b}^* = G_1\mathbf{S}^+ + G_2(\mathbf{S}^+\mathbf{\Omega}^+ - \mathbf{\Omega}^+\mathbf{S}^+) + G_3\left(\mathbf{S}^{+2} - \frac{1}{3}\{\mathbf{S}^{+2}\}\mathbf{I}\right)$. Multiplying the latter by the particle rate-of-strain tensor and taking the trace by invoking the two-dimensional property for cubic terms leads to write $b^*_{p,ij}S^+_{p,ij} = G_1 S^+_{p,ij}S^+_{p,ij} = G_1\eta_1$ (Girimaji, 1996). According to the definition of the production of the RUM kinetic energy by shear, $-\{\mathbf{R}^*\mathbf{S}^*\}$, and to the expression of G_1 (36), in the simplest case N should be taken as positive. In this study both the 2D and the 3D-A forms will be assessed. For both we will use the same second-order polynomial in N (34). Hereinafter this model will be referred to as 2ΦEASM2.

4.5. Model correction

In Sections 4.2 and 4.4.3 it has been shown, with restriction to two-dimensional flows, that a reverse sign in the energy exchange is related to the sign of the coefficient G_1 which is the same of the scalar quantities $\{\mathbf{R}^*\mathbf{S}^*\}$ and $\{\mathbf{b}^*\mathbf{S}^*\}$. This sign was shown to be negative in turbulence, in the domain of the applicability of the "weak-equilibrium" assumption (Girimaji, 1996). Instead, for the dispersed phase interacting with turbulent flows, it is usual to have a reverse exchange of energy from the RUM to the mesoscopic contribution (Moreau et al., 2010) which corresponds to a reverse sign of the first-order approximation coefficient. The model 2ΦEASM1 cannot predict such a state since the term $\{\mathbf{b}^*\mathbf{S}^*\}$ is modeled in that special case in which the two tensors $\mathbf{R}^*$ and $\mathbf{S}^*$ behave as in axisymmetric contraction and expansion respectively (negative sign) being observed as the most probable state. The models 2ΦEASM2 admits instead both positive and negative signs of G_1 since the solution is obtained by means of a polynomial in N which is depressed to a pure quadratic equation. As we have no additional information, we first choose the most probable sign on the base of the above considerations. In Section 4.2 it has been shown that the sign of the third invariant of $\mathbf{S}^*$ may be used to reproduce a reverse sign into model AXISY in that special case in which this is due to a change of state, from expansion to contraction, of the particle rate-of-strain tensor. In this section we will use the same quantity for modeling reverse energy exchanges in 2ΦEASM models. Its pertinence will be checked in Section 6. Accounting for the correction, Eq. (32) corresponding to the model 2ΦEASM1 is replaced by $-2\{\mathbf{b}^*\mathbf{S}^*\} = -2sign(III_S)\left(\frac{2}{3}\right)^{1/2}II_S^{1/2}$, and the quantity N (34) corresponding to the models 2ΦEASM2 by $N = -sign(\eta_3)\sqrt{2\eta_1 + 2\eta_2}$. III_S and η_3 are dimensional or dimensionless invariants, depending on the model. Besides the model AXISY, also 2ΦEASM1 and 2ΦEASM2 will be assessed with and without correction. When accounting for the correction, models will get the notation -C.

4.6. Characteristic timescale analysis

In Section 4.1 the viscosity model VISCO was recalled. This model assumes that the deviatoric RUM and the particle rate-of-strain tensors are related by a linear relationship through an eddy viscosity which uses the particle relaxation time as a typical timescale. This assumption may be compared to the fundamental hypothesis of the kinetic theory of dilute gases which is at the origin of the constitutive relation for Newtonian fluids. It involves the molecular motion adjusts rapidly to the change imposed by the local strain. Hence, for similarity, the basic assumption from which the viscosity model arises is violated when the ratio between the particle relaxation time and the mesoscopic strain timescale is large, i.e. $\tilde{\tau}_p S > 1$. This ratio is classically referred to as Knudsen number. The question about the domain of validity of a local eddy-viscosity assumption for large values of such a number, was already raised by Sakiz and Simonin (1998) and Simonin et al. (2002). In fact, when the strain is high, models which use the particle relaxation time as a typical timescale have little chance to work, in particular at large particle inertia. In order to address the question of the timescales, the two viscosity models presented in this manuscript are here compared. The models VISCO and AXISY are, respectively,

$$\delta R^*_{p,ij} = -\frac{2}{3}\tilde{\tau}_p\delta\theta_p S^*_{p,ij} \quad \text{and} \quad \delta R^*_{p,ij} = -II_b^{1/2}2\delta\theta_p\frac{S^*_{p,ij}}{S}. \tag{37}$$

It is easy to recognize that the difference resides in the two different timescales used by the models, that is $\tilde{\tau}_p/3$ versus $II_b^{1/2}/S$. In the one-component limit state, the relation between the times may be rewritten as

$$\tilde{\tau}_p \to \sqrt{6}S^{-1} \tag{38}$$

showing that VISCO and AXISY are viscosity-like models using two different timescales $\mathcal{F}(\tilde{\tau}_p)$ and $\mathcal{F}(S^{-1})$, respectively. The 2ΦEASM models, arisen from an assumption of equilibrium of anisotropy, also use $\mathcal{F}(S^{-1})$ as a typical timescale. It should be noted that these models are independent of the quantity which is used for the non-dimensionalization of the tensors. Their timescale is characterized by the dimensional term $|2\{\mathbf{b}^*\mathbf{S}^*\}|^{-1}$ which is $\sim S^{-1}$ in axisymmetric sheared flows. Finally, the quadratic approximation QUAD is characterized by the particle response time $\mathcal{F}(\tilde{\tau}_p)$. As discussed in the introduction of this section, models which use $\mathcal{F}(\tilde{\tau}_p)$ have little chance to work at high Knudsen numbers. This is why an alternative quadratic approximation using $\mathcal{F}(S^{-1})$ is suggested and presented in Section 4.7.

4.7. "Rescaled" quadratic algebraic approximation

Eq. (38), which relates the timescales of the two viscosity models, is here used to construct a new non-linear viscosity model based on the derivation proposed by Zaichik (2009) and presented in Section 4.3. Replacing $\tilde{\tau}_p$ with the new timescale and applying the same iteration procedure for which the second-order approximation is obtained by using the first-order approximation, the new model takes the form

$$\delta R^*_{p,ij} = -2\left(\frac{2}{3}\right)^{1/2}\delta\theta_p\frac{S^*_{p,ij}}{S} + \frac{2\delta\theta_p}{S^2}\left(S^*_{p,ik}\frac{\partial\tilde{u}_{p,j}}{\partial x_k} + S^*_{p,jk}\frac{\partial\tilde{u}_{p,i}}{\partial x_k} - \frac{2}{3}S^*_{p,mn}\frac{\partial\tilde{u}_{p,m}}{\partial x_n}\delta_{ij}\right). \tag{39}$$

If the particle inertia is not small enough, the assumption of small parameter $\epsilon = \tilde{\tau}_p S$ allowing to justify the expansion procedure is no longer valid. Accounting for the new timescale makes it possible to extend the range of applicability of the model. The above expression, at the first order, leads to the viscosity model AXISY if the one component limit state and a positive viscosity are used. Eq. (39) written in term of anisotropy, using dimensionless (by $II_S^{1/2}$) tensors, is $\mathbf{b}^* = -\left[\left(\frac{2}{3}\right)^{1/2} - \frac{2}{3}\{\mathbf{S}^+\}\right]\mathbf{S}^{*+} - (\mathbf{S}^{*+}\mathbf{\Omega}^+ - \mathbf{\Omega}^+\mathbf{S}^{*+}) + 2\left(\mathbf{S}^{*+2} - \frac{1}{3}\{\mathbf{S}^{*+2}\}\mathbf{I}\right)$. The latter has the same form as the 2ΦEASM models previously presented (asterisks are kept here to distinguish the traceless dimensionless tensor $\mathbf{S}^{*+}$ from the trace of the non-traceless dimensionless tensor $\{\mathbf{S}^+\}$ appearing in this equation). Indeed, comparing the rescaled quadratic approximation developed in this section with the two-dimensional approximation of the explicit solution given in Section 4.4.3 leads to write $G_1 = -[(2/3)^{1/2} - 2/3\{\mathbf{S}^+\}]$, $G_2 = -1$ and $G_3 = 2$. However, it should be noted that in order to be consistent with the anisotropy-equilibrium assumption and the non-dimensionalization of the tensors by $II_S^{1/2}$, the above coefficients should be divided by 2. In such a case, Eq. (39) would be a particular case of the 2D form of 2Φ EASM2. The assessment of

the model have shown that a coefficient 0.5 is indeed appropriate. Hereinafter, Eq. (39) divided by 2 will be referred to as QUAD-MOD.

A summary of the models investigated by the present study, including their main assumption, characteristic timescale and treatment of the reverse energy exchange is given in Table 3.

5. Numerical simulations: Eulerian–Lagrangian DNS for building the particle Eulerian database

Fig. 1 is a stylized picture showing the numerical configuration used in this study. The slab is a temporal turbulent planar jet laden with small and heavy particles (Vermorel et al., 2003). The simulation domain is a cube of length size $L_{box} = 2\pi L_{ref}$ and mesh composed of 128^3 or 256^3 cells, depending on the simulation. The initial gas velocity has hyperbolic-tangent mean profile supplemented with statistically homogeneous and isotropic velocity fluctuations. The fluid initial set up is summarized in Table 4. The turbulence is initialized by a Passot–Pouquet spectrum (Passot and Pouquet, 1987) setting the energetic lengthscale to $Le = 0.0637 L_{box}$. A certain amount of experimentations led to chose this value. Results showed that larger values of Le lead to a decaying turbulence. Instead, the energetic lengthscale employed in this study, being it close to the large scales of the turbulent jet, makes it possible to develop additional turbulent velocity fluctuations from the mean shear. As a consequence, at the end of the simulations, in the high-shear zones of the jet, the intensity of the turbulence is doubled. For the 128^3 DNS, at the final time, the Reynolds number based on the turbulent dissipation lengthscale, $Re_{L_E} = \left(q_f^2\right)^2/(\epsilon_f \nu_f)$, is $\mathrm{Re}_{LE} \sim 80$ at the center of the jet and almost the double in the zones of high shear. For the 256^3 DNS, it is $\mathrm{Re}_{LE} \sim 200$ at the center of the jet and up to three-time as much in the zones of high shear. q_f^2 and ϵ_f are fluid turbulent kinetic energy and dissipation computed by planar averages; ν_f is the fluid kinematic viscosity. Within the slab, of width $d = 0.25 L_{box}$, particles are randomly embedded at the same mean velocity as the carrier flow and zero fluctuations, and their number ($\mathcal{N}_S$) is large enough to permit mesoscopic fields

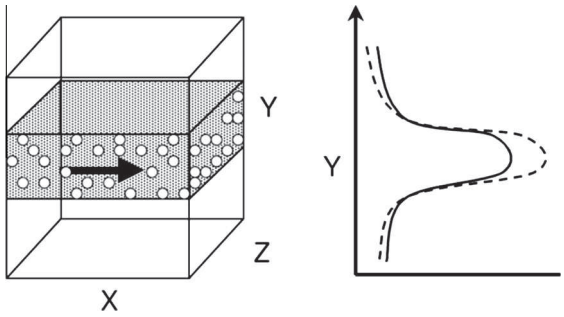

Fig. 1. Stylized picture of the particle-laden slab by Vermorel et al. (2003).

Table 4
Turbulence parameters at the time $t = 0$.

Simulation	128^3 DNSs	256^3 DNS
Jet mean velocity	$U_f = 0.15 u_{ref}$	$U_f = 0.15 u_{ref}$
Turbulence intensity	$I_f = 0.10$	$I_f = 0.10$
Kinematic viscosity	$\nu_f = 1.82\ 10^{-4}\ u_{ref} L_{ref}$	$\nu_f = 5\ 10^{-5}\ u_{ref} L_{ref}$
Turbulent kinetic energy	$q_f^2 = 3.37\ 10^{-4}\ u_{ref}^2$	$q_f^2 = 3.37\ 10^{-4}\ u_{ref}^2$
Dissipation	$\epsilon_f = 3.78\ 10^{-5}\ u_{ref}^3/L_{ref}$	$\epsilon_f = 1.04\ 10^{-5}\ u_{ref}^3/L_{ref}$
Kolmogorov lengthscale	$\eta = 0.02 L_{ref}$	$\eta = 0.0105 L_{ref}$
Dissipation lengthscale	$L_E = 0.165 L_{ref}$	$L_E = 0.595 L_{ref}$
Kolmogorov timescale	$\tau_K = 2.19 L_{ref}/u_{ref}$	$\tau_K = 2.19 L_{ref}/u_{ref}$
Dissipation timescale	$T_E = 8.92 L_{ref}/u_{ref}$	$T_E = 32.40 L_{ref}/u_{ref}$

calculation (13 million particles for the 128^3 DNSs, 210 million particles for the 256^3 DNS). The sample size $\mathcal{N}_S$ approximates the statistical population of particles over all the particle realizations $\mathcal{H}_p$ conditional on one given flow realization $\mathcal{H}_f$ (Kaufmann et al., 2008). The larger is the sample size the more accurate is the approximation. Numerical simulations are performed using the Eulerian–Lagrangian NTMIX3D-2Φ code. This code solves the compressible NS equations in dimensionless form by a third order Run-

Table 3
Summary of the models investigated by the present study and their main assumption, characteristic timescale and capability to reproduce reverse energy exchange. The linear/nonlinear nature of the constitutive relations is defined in terms of particle velocity gradient. 2ΦEASM2 is also tested using the 2D approximation for N together with a ten-tensors basis (referred to as 3D-A solution).

Model	Main assumption	Constitutive Relation	Time scale	Reverse energy exchange
VISCO	Equilibrium of stresses + light anisotropy (first-order approximation)	Linear	$\mathscr{F}(\tilde{\tau}_p)$	not allowed
QUAD	Equilibrium of stresses + quadratic approximation based on first-order (VISCO) approximation	Non Linear		allowed
AXISY	Axisymmetric particle stress and strain tensors + stress one-component limit	Linear	$\mathscr{F}(S^{-1})$	not allowed
AXISY-C				allowed through correction enabling negative viscosity
QUAD-MOD	Equilibrium of stresses + quadratic approximation based on first-order (AXISY) approximation	Non Linear		allowed
2ΦEASM1	Equilibrium of anisotropy + 2D approximation + axisymmetric tensors and stress one-component limit	Non Linear		not allowed
2ΦEASM1-C				allowed through correction of the first-order coefficient
2ΦEASM2	Equilibrium of anisotropy + 2D approximation	Non Linear		partially allowed by quadratic terms
2ΦEASM2-C				allowed through correction of the first-order coefficient

ge–Kutta time stepping and a sixth-order compact finite-difference scheme on a Cartesian grid (Lele, 1992). The Lagrangian particle tracking is ensured by a third order Runge–Kutta scheme. The interpolation of the turbulent fields at the particle location is performed by a third-order Lagrange polynomial algorithm. Periodic boundary conditions are applied to both the carrier and the dispersed phase in all the directions due to the contained jet expansion. The computations are parallelized using three-dimensional domain decomposition and message passing. Eight Eulerian–Lagrangian 128^3 DNSs are carried out. The point-particle Lagrangian approach used in this study is described in Appendix A. Simulations correspond to a Stokes number, St, ranging between $\sim$0.1 and $\sim$10, computed over a characteristic macroscale of the turbulence seen by the particles $T_{f@p}$ (Deutsch and Simonin, 1991). Only one 256^3 DNS is instead performed and it corresponds to St of about unity. The technique employed for estimating the Stokes numbers as well as the definition retained in this study are given in Appendix B. For all the simulations the particle diameter is set to $d_p = 0.0005L_{ref}$ and the particle-to-gas density ratios is chosen such to obtain the wished Stokes numbers. From such deterministic simulations, a particle Eulerian database is obtained using the projection procedure suggested by Moreau et al. (2010), Kaufmann et al. (2008). The "exact" particle Eulerian fields are then used for an *a priori* analysis purpose.

6. Results of the *a priori* analysis

The analysis presented in this section, and in general when not mentioned, refers to the 128^3 DNSs; results corresponding to the 256^3 DNS are shown in Appendix C. Statistics are computed, using the Eulerian database, over all the planes of the slab; however, for the sake of synthesis, results are shown for that planes considered representative of the jet and referred to as "the centre" and "the periphery". The former corresponds to the plane in the middle of the box ($y = 0$), the latter represents a portion of the slab located in the upper (lower) part of the box, of y (dimensionless) coordinates ranging between 0.6 and 0.8 (-0.6 and -0.8) being $y = \pm 0.8$ the periphery of the jet at the initial time. This portion of the slab is chosen in order to ensure particle sample sizes large enough to provide accurate statistics. Results which are shown as a function of the Stokes number are computed by averaging Eulerian fields over planes and over the six last times of each simulation. Times are shown as a function of $T^r_{f@p}$ which represents the timescale of the turbulence seen by the particles of a simulation of reference ($St \sim 1$, as explained in Appendix B). The analysis is performed at both tensor and scalar levels (Clark et al., 1979). At the tensor level, the assessment is made over each component of the deviatoric RUM by comparison between actual and modeled mean profiles computed by density-weighted averaging the Eulerian fields over the homogeneity planes of the planar jet. At the scalar level, the models' accuracy is evaluated through the assessment of the predictions of the RUM kinetic energy production (14). This term accounts for both the productions by shear and compression. As only the deviatoric-RUM closures are investigated, the only contribution by shear is retained. The latter is referred to as $\tilde{n}_p P^*_{RUM}$. Splitting in mean and fluctuating velocity-gradient contributions, it is

$$\tilde{n}_p P^*_{RUM} = \tilde{n}_p \overline{P}^*_{RUM} + \tilde{n}_p P^{*\prime}_{RUM} = -\tilde{n}_p \delta R^*_{p,ij} \frac{\partial \overline{U}_{p,i}}{\partial x_j} - \tilde{n}_p \delta R^*_{p,ij} \frac{\partial \tilde{u}'_{p,i}}{\partial x_j}. \quad (40)$$

The quantity $\tilde{n}_p P^*_{RUM}$ is initially chosen for assessing the models. Its right prediction is of extreme importance as the mechanisms of inter-particle collision and coalescence are functions of the local amount of the RUM kinetic-energy intensity which relies on $\tilde{n}_p P^*_{RUM}$. However, an analysis carried out by Février et al. (2005) and the authors has shown that only the turbulent-velocity gradient contribution, $\tilde{n}_p P^{*\prime}_{RUM}$, is responsible for the energy transfer from mesoscopic to the RUM component and that, in addition, its local magnitude prevails on the mean-velocity gradient contribution. For this reason, $\tilde{n}_p P^{*\prime}_{RUM}$ needs to be carefully evaluated. Indeed, a kinetic-energy transfer rate which is badly predicted may dramatically affect the numerical simulation. For example, an overestimation could give rise to re-laminarization phenomena as that observed by Riber (2007) when performing Eulerian–Eulerian simulations of a mean-sheared particle-laden turbulent jet. For this reason, the models will be assessed over the quantity $\tilde{n}_p P^{*\prime}_{RUM}$ as well. At the scalar level, the accuracy of each model is evaluated by means of correlation coefficients computed between actual (A) and modeled (M) quantities as $C(A,M) = (\langle AM\rangle - \langle A\rangle\langle M\rangle)/\sqrt{(\langle A^2\rangle - \langle A\rangle^2)(\langle M^2\rangle - \langle M\rangle^2)}$ and by the magnitude ratio between actual and modeled mean quantities $\mathcal{M}(A,M) = \langle A\rangle/\langle M\rangle$ (where brackets denote averages over xz-planes). The latter represents an ideal multiplicative coefficient which should be accounted for into the model in order to predict the exact mean magnitude. Point-wise functions, as PDFs, are also used for the investigation of the model accuracy.

6.1. Approximation of complex solutions in 2ΦEASM2 and model correction

Through the *a priori* analysis, we first investigate the legitimacy of the assumption used in Section 4.4.3. In that section we developed a model, 2ΦEASM2, as an explicit solution of the novel implicit and non-linear equation system (27). 2ΦEASM2 was obtained

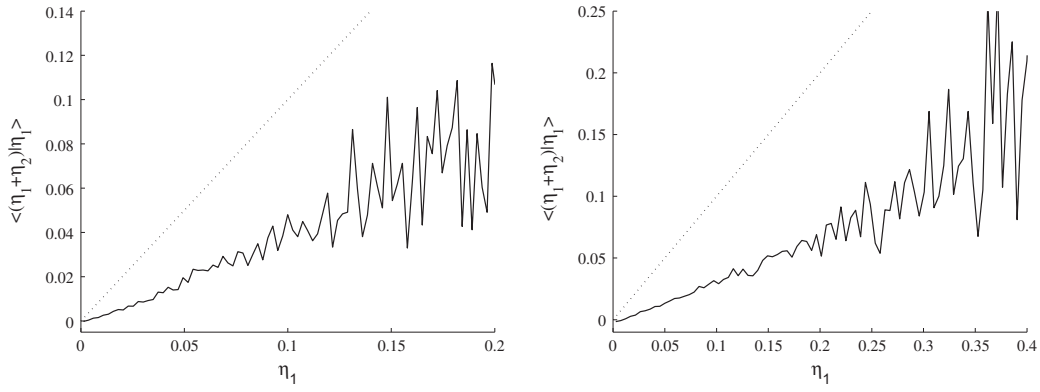

Fig. 2. Average of the quantity $\eta_1 + \eta_2$ conditional on η_1, for the simulation corresponding to $St \sim 3$, at the centre (left) and at the periphery (right) of the jet, at the time $t = 6.2T^r_{f@p}$.

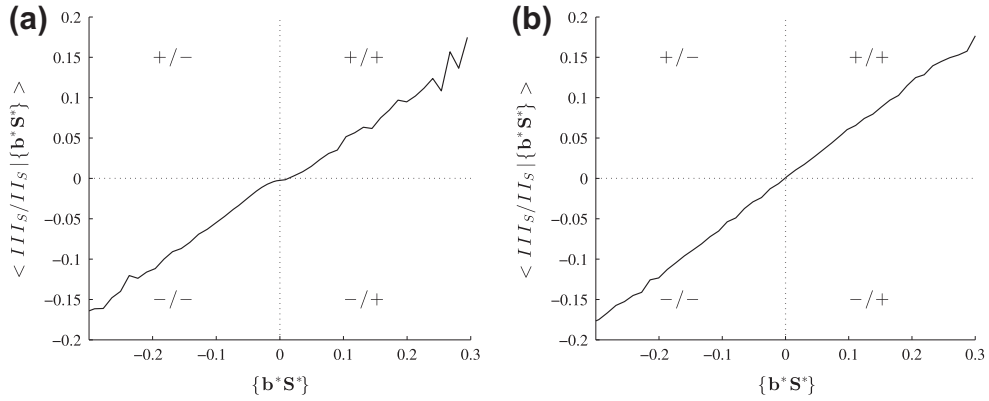

Fig. 3. Conditional average of normalized III_S on the quantity $\{\mathbf{b}^*\mathbf{S}^*\}$, corresponding to the simulation $St \sim 2$ (a) and $St \sim 7$ (b), at the periphery of the jet, at the time $t = 6.2T^r_{f@p}$.

using a technique (Wallin and Johansson, 2000) which involves the solution of a polynomial in N which, in absence of collisions, reduces to the pure quadratic equation $N^2 = 2\eta_1 + 2\eta_2$. In order to ensure real solutions, we introduced the approximation $N = 0$ in correspondence of $(\eta_1 + \eta_2) < 0$. Fig. 2 shows the average of $(\eta_1 + \eta_2)$ conditional on the invariant η_1, over two planes of the slab, for the simulation corresponding to $St \sim 3$. Results indicate that negative values involving complex solutions are mainly concentrated in zones where the two invariants η_1 and η_2 are very small and the approximation $N = 0$ is therefore legitimate. Second, we check the appropriateness of the sign of the third invariant III_S introduced in Sections 4.2 and 4.5 (and referred to as "correction" - C) in order to enable the models AXISY, 2ΦEASM1 and 2ΦEASM2 to predict reverse energy exchanges. The pertinence of the correction is evaluated correlating the sign of the third invariant III_S with the sign of the quantity $\{\mathbf{b}^*\mathbf{S}^*\}$ by using the conditional average. Results of the simulations corresponding to the Stokes numbers $St \sim 2$ and $St \sim 7$ are displayed in Fig. 3. A strong correlation between the signs of the two quantities is found, which motivates the use of the correction in the models.

6.2. 2D versus 3D-A 2ΦEASM2

Before to assess all the models by comparing their predictions, 2D and 3D-A forms of 2ΦEASM2 are investigated. For the sake of brevity, only the corrected model is presented and only at the tensor level over the main components. Fig. 4 shows the mean profiles of the normal, $\delta R^*_{p,11}$, and the shear, $\delta R^*_{p,12}$, components of the deviatoric RUM for the simulation corresponding to $St \sim 1$, as an example. The two components are assessed using both the 2D and the 3D-A forms of 2ΦEASM2-C. Results show that despite the improvement of the predictions obtained by using the three-dimensional approximation, the latter cannot ensure stable solutions since local singularities occur. Such singularities are due to the local null values of the denominator Q (Eq. (35)) involved in the definition of the ten coefficients (Table 2) which multiply the integrity basis composed of the ten tensors recalled in Table (1). In order to use the 3D-A form of the model, a regularization procedure or additional approximations are necessary. This concern is not addressed by this study as the 2D form gives satisfactory results. It is conjectured that when in the presence of a mean shear, the local agitation may be larger in the streamwise direction with respect to the others and this may explain the success of a 2D assumption. However, it should be stressed that the dispersed phase is locally fully three dimensional since the particle fields are non-null in all the three directions. An effort on the modeling for improving predictions in three-dimensional flows could be very effective. In turbulent flows, a 3D approximation using a ten-tensor basis together with an approximate anisotropy equation was derived by Wallin and Johansson (2000). They used argument about the value of the coefficients multiplying high-order terms in the anisotropy equation in order to neglect one of them as already

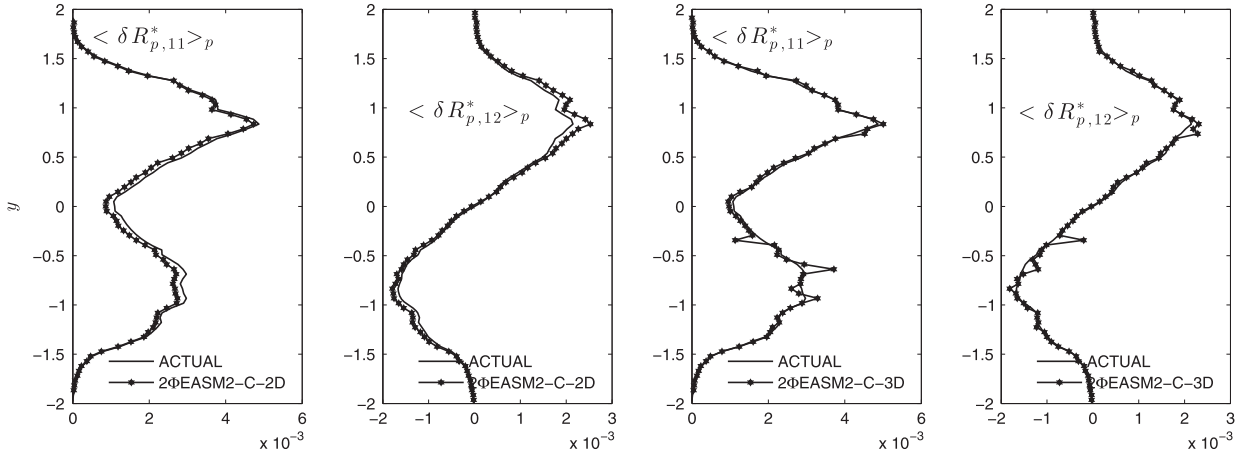

Fig. 4. Mean deviatoric RUM stresses $\delta R^*_{p,11}$ and $\delta R^*_{p,12}$, for the simulation corresponding to $St \sim 1$, at the time $t = 6.2T^r_{f@p}$. Actual stresses (solid line) are compared with predictions (line with symbols) obtained using the 2D (two graphics on the left) and the 3D-A (two graphics on the right) forms of 2ΦEASM2-C.

suggested by Taulbee (1992). In the dispersed phase where the anisotropy equation is devoid of variable coefficients, a similar approximation needs an analysis of the influence of each term on the predictions in order verify the legitimacy of an approximate anisotropy equation. An alternative 3D approximate solution could be derived using an incomplete tensor basis including cubic or quartic terms combined with the full anisotropy equation. Moreover, alternative techniques of derivation of an explicit solution using an incomplete basis, as a Galerkin method (Jongen and Gatski, 1998) or a least-squares method (Grundestam et al., 2005) could be adopted. This concern represents a challenge and is left to a future work. Hereinafter, 2ΦEASM2 (with or without correction) will refer to the 2D form of the model.

6.3. Tensor-level model assessment

A first assessment of the deviatoric-RUM models developed by the present study is given by comparing actual and modeled mean profiles corresponding to the numerical simulation $St \sim 3$. In fact, as these results are found scarcely affected by the particle inertia at tensor level, the selected numerical simulation gives valuable information which may be reasonably generalized to all the Stokes number simulations (differences between Stokes-number predictions are mainly found on the shear component, not shown). Fig. 5(a) displays the predictions obtained using the linear models VISCO, AXISY and AXISY-C. Results show the inability of these models to reproduce the normal stresses. AXISY gives even worse results than VISCO. The use of the correction, i.e. AXISY-C, certainly improves the predictions of the normal stresses but does not remove this deficit. Further, the shear stress results to be slightly underestimated by AXISY-C. Nevertheless, it is worth of note that the two axisymmetric models reproduce decisively better the shear component with respect to VISCO which largely overestimates it. The poor predictions over the normal stresses of the axisymmetric models are a manifestation of the limits of an axisymmetric assumption for particle rate-of-strain tensor. Contrary to the RUM tensor for which the one-component limit behavior is found decisively prevalent (as also proved by the magnitude of the normal deviatoric RUM components), an axisymmetric configuration for the particle rate-of-strain tensor is instead one of the local and instantaneous state, even if the most probable, among the others observed by numerical simulations. Other states, as the plane shear, cannot accurately support a linear relationship for the dispersed phase. Predictions from the quadratic approximations are given by Fig. 5(b). Here, the mean profiles of QUAD are shown multiplied by a factor 0.05. Results indicate that this model hugely overestimates (of about two orders of magnitude) the stresses at any level. It is conjectured that the particle relaxation time does not represent the correct timescale in the constitutive relationship which uses the particle rate-of-strain tensor as a basis. As already discussed in Section 4.6, models which use $\mathcal{F}(\tilde{\tau}_p)$ as a timescale may only be effective for Knudsen numbers smaller than unity and they cannot be used at large particle inertia. The inappropriateness of the timescale is more evident in QUAD than in VISCO because the former uses powers of τ_p in the series expansion. QUAD-MOD is the proof of such a conjecture. This model, which uses $\mathcal{F}(S^{-1})$ as the timescale, slightly overestimates the shear component reproducing very well the normal stresses. Results of the predictions obtained using the models which arise from a similarity assumption, i.e. 2ΦEASM, are displayed in Fig. 5(c and d). Examination of these figures shows that 2ΦEASM1 underestimates the magnitude of all the deviatoric-RUM components and that the use of the correction only slightly improves the predictions. Satisfactory results are instead provided by 2ΦEASM2 (Fig. 5(c)) in particular when the correction is used (Fig. 5(d)). It is worth of note the excellent agreement between the components of modeled by 2ΦEASM2-C and actual stresses. As a further evidence of the excellent performance of this model, mean profiles are assessed for the simulation corresponding to $St \sim 7$ and results shown by Fig. 6.

6.4. Scalar-level model assessment over $\tilde{n}_p P^*_{RUM}$

Fig. 7(a) shows the models' assessment at the scalar level over the quantity $\tilde{n}_p P^*_{RUM}$. Fig. 7(b) shows the assessment of that models which use the correction introduced in Section 4.5. Both the figures display correlation coefficients computed as detailed above. Comparing VISCO to AXISY (or QUAD to QUAD-MOD), arising from the same formalism but using two different timescales, no large differences are found in terms of correlation coefficients. Instead, strong differences are found when comparing linear models (VISCO and AXISY) to non-linear models (QUAD and QUAD-MOD). QUAD and QUAD-MOD provide higher correlation values, scarcely affected by the particle inertia. QUAD-MOD gives even better results corresponding to correlation coefficients as well as or larger than 0.9. Instead, the accuracy of VISCO and AXISY decreases as the particle inertia increases, leading to very poor correlations at large Stokes numbers. It is conjectured that such a decrease of the model accuracy as the particle inertia increases is mainly due to the increasing of the reverse energy exchange from the RUM to the mesoscopic contribution rather than to a failure in the alignment assumption. Linear models which use a positive viscosity cannot indeed predict such reverse energy exchanges and they are doomed to fail at large Stokes numbers. The evidence of such a conjecture is given by the predictions of the linear model which uses both positive and negative viscosities, namely AXISY-C (Fig. 7(b)). Its results appear quite insensitive to the particle inertia. Concerning the 2ΦEASM models, results indicate that globally they give satisfactory predictions and that, as expected, 2ΦEASM2 performs better than 2ΦEASM1 since it represents a self-consistent explicit solution of the 2ΦASM closure (Eq. (27)). It is noteworthy the agreement of these models with the actual local quantity when the correction is used. Among all the models, 2ΦEASM2-C is that which best reproduces the local production of the RUM particle kinetic energy. Its results are excellent and give correlation coefficient close to unity (perfect agreement). In Fig. 8, the magnitude ratios between actual and predicted mean productions, $< P^*_{RUM} >_p$, are displayed. Looking at the results, the differences between models are surprising. Models VISCO and QUAD which are based on the particle relaxation timescale $\mathcal{F}(\tilde{\tau}_p)$, dramatically loose their ability to predict the good magnitude of the mean production when the particle inertia increases; comparing the largest with the smallest Stokes-number simulation, a decrease up to three orders of magnitude is observed. This great variability makes these models not adequate to predict the RUM agitation, in particular when in the presence of a locally varying particle Stokes number as, for instance, in evaporating or polydisperse particle-laden turbulent flows. Moreover, large particle inertia are also prohibitive if a well calibrated "very small" coefficient is not accounted for into these models. Unfortunately, results obtained at the tensor level, see e.g. the model VISCO, have shown that accounting for a small coefficient ($\ll 1$) would reduce the magnitude of the stresses, making the model fail at the tensor level. Results give the evidence that the models which use the inverse of the particle strain $\mathcal{F}(S^{-1})$ as a typical timescale are less sensitive to the particle inertia. In addition results indicate that the models which are able to reproduce both positive and negative value of the local quantity $\tilde{n}_p P^*_{RUM}$, as for instance the models which use the correction, give the best agreement. An ideal prediction should reproduce magnitude ratios equal to unity regardless of the particle Stokes number. In order to conclude the assessment of the model accuracy over $\tilde{n}_p P^*_{RUM}$, the PDFs of this local scalar quantity are investigated. They are as-

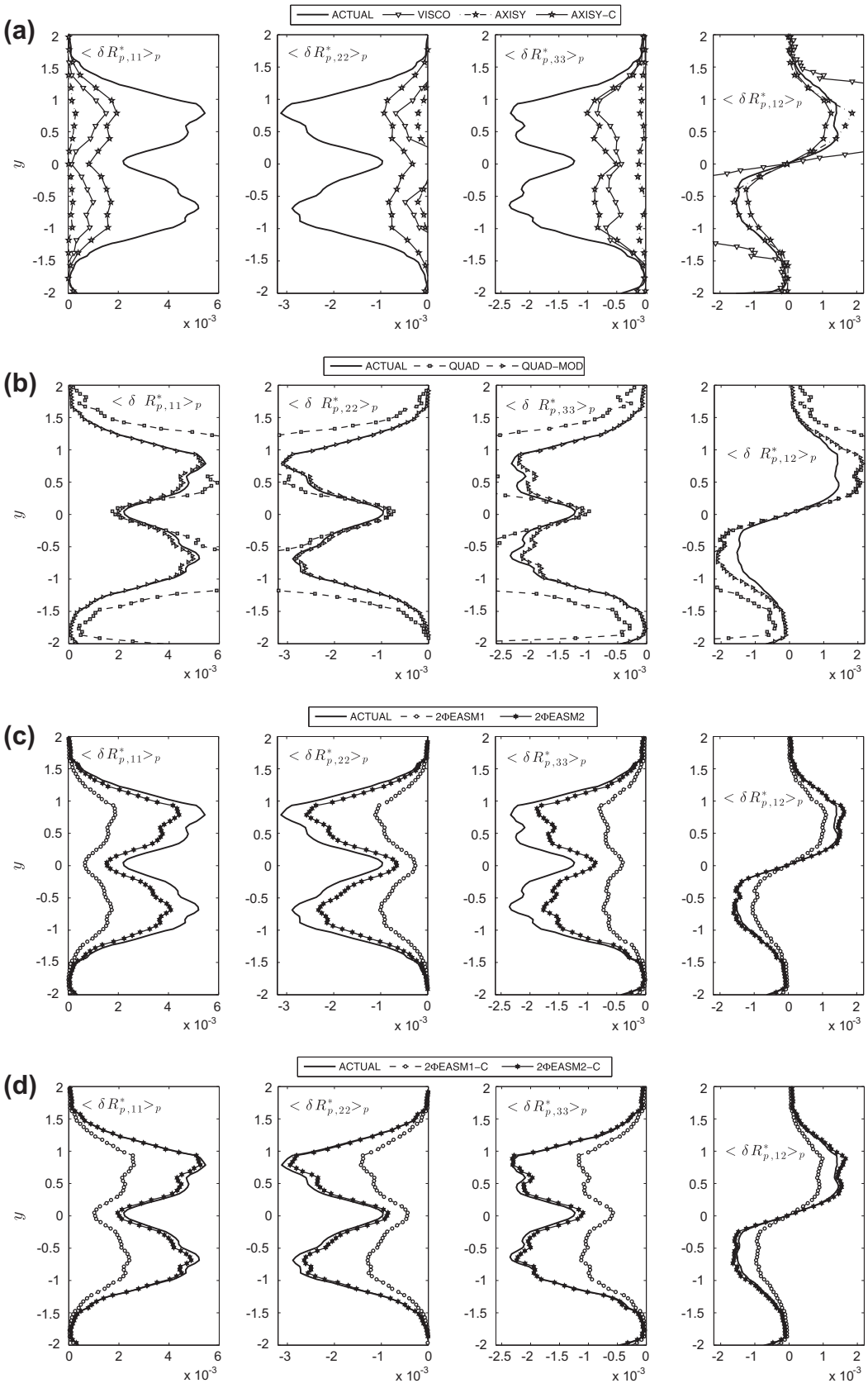

Fig. 5. Profiles of actual (solid line) and modeled (lines with symbols) mean deviatoric RUM stresses, for a simulation corresponding to $St \sim 3$, at the time $t = 6.2T^r_{f@p}$. Stresses are normalized by the square mean velocity of the jet at $t = 0$.

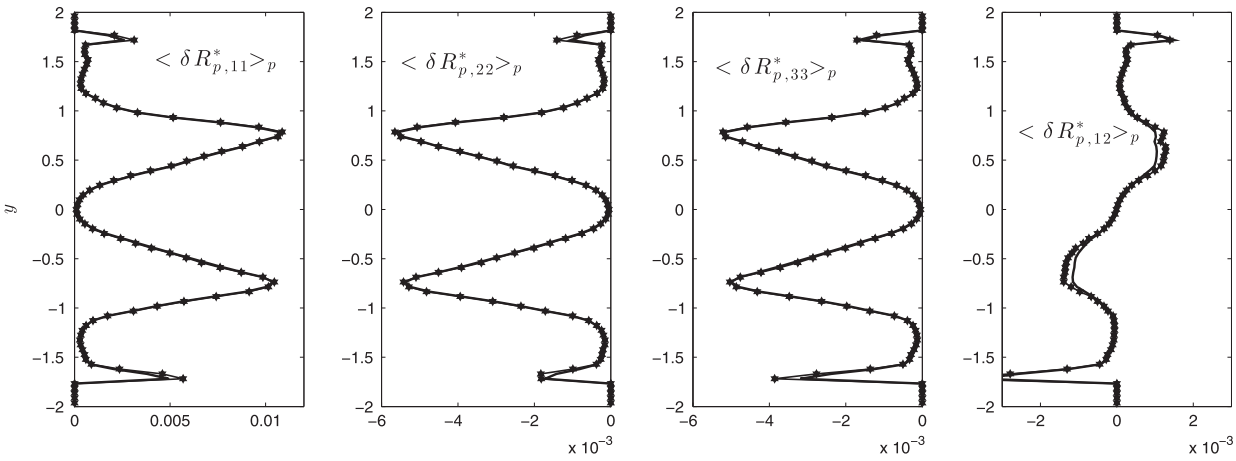

Fig. 6. Profiles of actual (solid line) and modeled by 2ΦEASM2-C (lines with symbols) mean deviatoric RUM stresses, for a simulation corresponding to $St \sim 7$, at the time $t = 6.2T^r_{f@p}$. Stresses are normalized by the square mean velocity of the jet at $t = 0$.

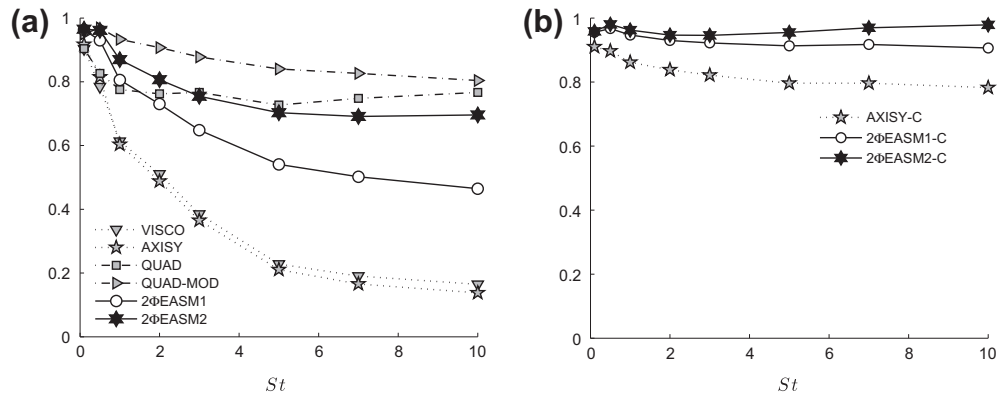

Fig. 7. Correlation coefficients between the actual and the modeled scalar quantity P^*_{RUM}, at the periphery of the jet.

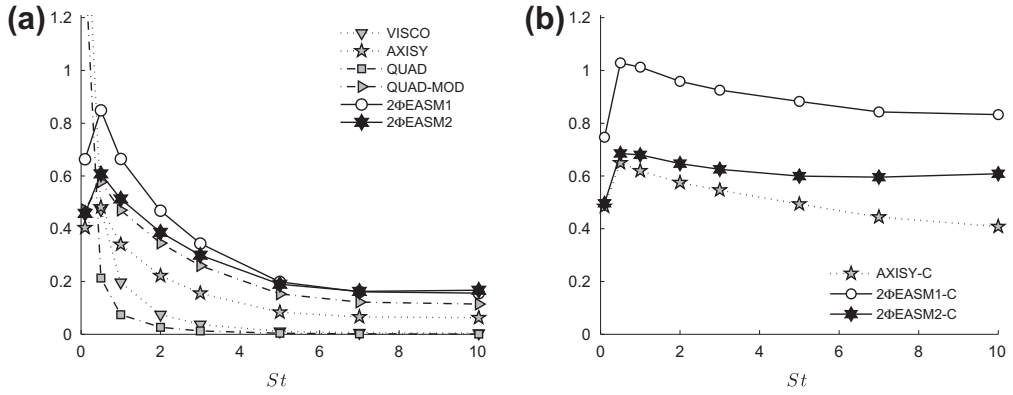

Fig. 8. Magnitude ratios between the mean actual and the mean modeled scalar quantity P^*_{RUM}, at the periphery of the jet.

sessed by multiplying the local value of the modeled $\tilde{n}_p P^*_{RUM}$ by the magnitude ratio computed from each model, and the results compared to the actual PDF; by this way, only the shape of the PDFs is investigated (Moreau, 2006). First, we check the predictions of all the models at one selected Stokes number ($St \sim 3$); they are displayed in Fig. 9. Results indicate that the two viscosity-like models, VISCO and AXISY, are not able to reproduce reverse energy exchanges, as expected. Similar behavior is found for 2ΦEASM1 which uses a positive production approximation (Eq. (32)) for the linearization of the 2ΦASM closure. Local negative values are instead provided by all the other non-linear models. It is interesting to note that the predictions by QUAD cover a larger range of negative values than QUAD-MOD, and that the predictions by QUAD-MOD, which uses the inverse of the particle strain as a time-scale, are very close to that of 2ΦEASM2. In order to check the influence of the model correction on the shape of the PDF, we specifically analyze that models for which the correction do apply. It is noteworthy the excellent agreement between exact and modeled quantities when the correction is used, as illustrated by Fig. 10. Among all the models, 2ΦEASM2-C gives the best local representa-

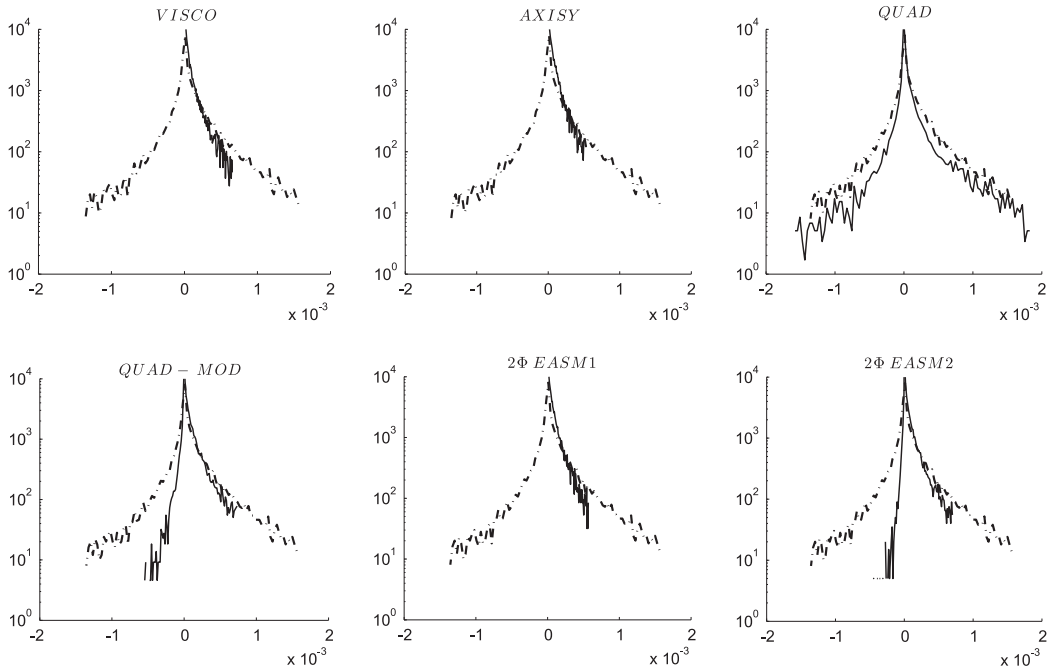

Fig. 9. PDFs of actual (dot-dashed line) and modeled (solid line) $\tilde{n}_p P^*_{RUM}$, for a simulation corresponding to $St \sim 3$. Models without correction, at the periphery of the jet, at the time $t = 6.2T^r_{f@p}$.

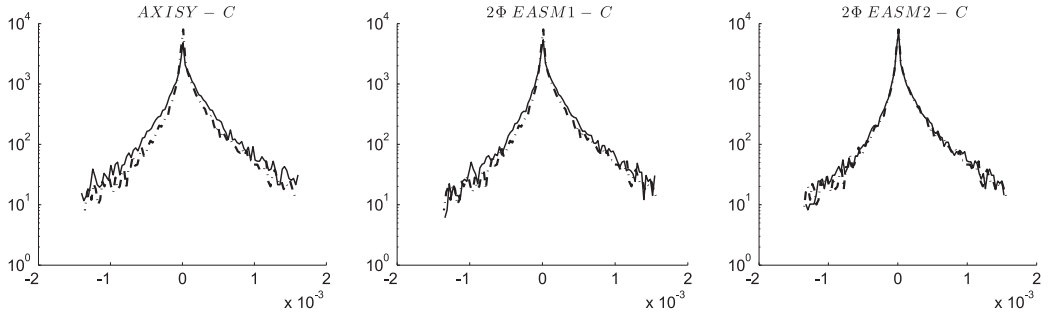

Fig. 10. PDFs of actual (dot-dashed line) and modeled (solid line) $\tilde{n}_p P^*_{RUM}$, for a simulation corresponding to $St \sim 3$. Models with correction, at the periphery of the jet, at the time $t = 6.2T^r_{f@p}$.

tion of $\tilde{n}_p P^*_{RUM}$ at this selected Stokes number. The assessment over different Stokes numbers (not shown for sake of brevity) points out that for some models as VISCO, QUAD and QUAD-MOD, the increase of the Stokes number worsens the predictions. A slight decrease of the model accuracy is also found for the models AXISY-C and 2ΦEASM1-C. An exception is the model 2ΦEASM2-C which gives excellent results, on the shape of the PDF, regardless of the particle inertia. This model has given proof of its ability to model the deviatoric RUM kinetic stress tensor at both scalar and tensor levels.

6.5. Scalar-level model assessment over $\tilde{n}_p P^{*\prime}_{RUM}$

Finally, the models' accuracy over the only fluctuating contribution of the RUM kinetic energy production, namely $\tilde{n}_p P^{*\prime}_{RUM}$, is investigated. This quantity is supposed to play a crucial role in the numerical simulations since it contributes to ensure the correct level of the mean dissipation rate (Février et al., 2005). Correlation coefficients (not shown for brevity) show that no noticeable difference is observed comparing these results to that obtained over the quantity $\tilde{n}_p P^*_{RUM}$. Instead, some significant differences are found when assessing the magnitude ratios at large Stokes numbers. This

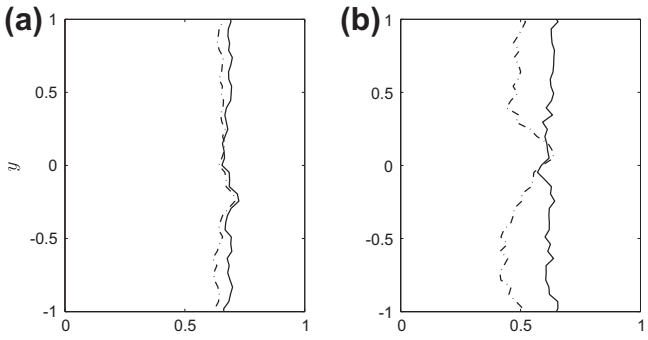

Fig. 11. Profiles of magnitude ratios between actual and modeled mean P^*_{RUM} (solid line) and actual and modeled mean $P^{*\prime}_{RUM}$ (dot-dashed line). Simulation corresponding to $St \sim 0.5$ (a) and $St \sim 3$ (b), at the time $t = 6.2T^r_{f@p}$. The model used is 2ΦEASM2-C.

parameter is an index of the ability of the models to reproduce exact mean magnitudes. As illustrated by Fig. 11, for the model 2ΦEASM2-C, results show that for moderate Stokes numbers (St ∼0.5 as an example) the predictions of the two quantities $\tilde{n}_p P^*_{RUM}$

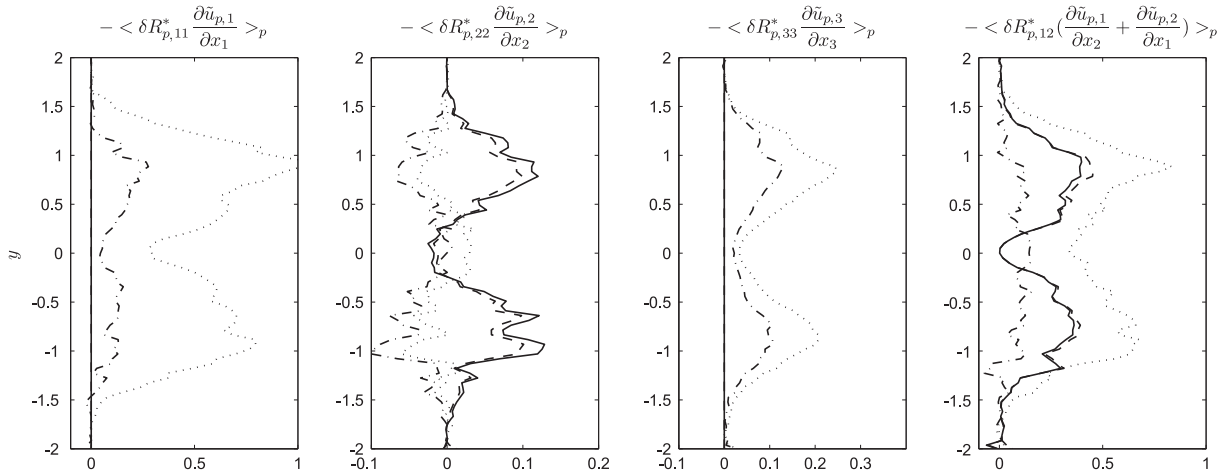

Fig. 12. Mean profiles of the main addends of the total production by shear $P^*_{RUM} = \overline{P}^*_{RUM} + P^{*\prime}_{RUM}$. Solid line: exact $<\overline{P}^*_{RUM}>_p$; Dashed line: modeled $<\overline{P}^*_{RUM}>_p$; Dot-dashed line: exact $<P^{*\prime}_{RUM}>_p$; Dotted line: modeled $<P^{*\prime}_{RUM}>_p$. Simulation corresponding to $St \sim 3$, at the time $t = 6.2T^r_{f@p}$. Productions are normalized by the fluid dissipation rate computed at the centre of the jet, $\epsilon_f(y = 0)$. The model used is 2ΦEASM2.

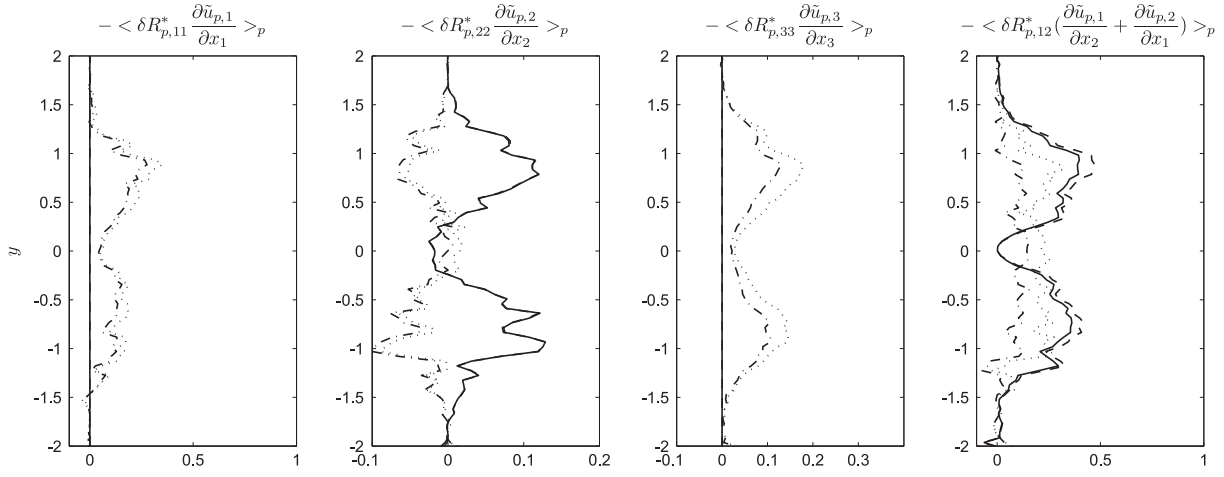

Fig. 13. Same caption as in Fig. 12. The model used is 2ΦEASM2-C.

and $\tilde{n}_p P^{*\prime}_{RUM}$ are nearly identical. For larger Stokes numbers (St ∼3 as an example) the difference becomes more noticeable but not yet dramatic, in particular if the model correction is used. For Stokes numbers even larger (not shown), the predictions of the mean magnitude progressively deteriorate at the periphery of the jet where, in contrast, the accuracy of some models remains excellent at the tensor level, almost irrespective of the particle inertia in particular over the normal components (Section 6.3). A crucial point of the modeling is that the two productions, by mean and fluctuating mesoscopic velocity gradients, do not have the same response to the modeling. In order to analyze this point more in detail, the profiles of the most relevant components of the RUM kinetic-energy production, decomposed in mean and fluctuating particle-velocity gradients, $\langle \overline{P^*}_{RUM} \rangle_p$ and $\langle P^{*\prime}_{RUM} \rangle_p$, are investigated. They are computed using the model which gives the best predictions, namely 2ΦEASM2, accounting or not for the correction; results for the simulation corresponding to St ∼3 are displayed in Figs. 12 and 13. Results show that for this Stokes number, 2ΦEASM2 overestimates the contributions which stem from the fluctuating velocity gradients, while it matches very well the contributions arising from the mean velocity gradients (Fig. 12). When the model correction is used (2ΦEASM2-C), predictions are strongly improved as illustrated by Fig. 13; however, a slight overestimation persists at this Stokes number. The overestimation is expected to increase with the particle inertia in high shear zones of the jet. The analysis at the tensor level have shown (Section 6.3) that even for large Stokes numbers, the mean deviatoric RUM kinetic stress tensor is successfully represented by the algebraic closures developed by the present study, but different strategies should be adopted to enable the models at the scalar level, i.e. to ensure the right level of the RUM particle kinetic energy. As the modeling of the RUM tensor depends on the accuracy of the RUM kinetic energy, if the latter is not well reproduced during the DNS, the model for the deviatoric RUM will fail. This problem is slightly smoothed in the framework of the LES, because of the filtering operation which acts to reduce the reverse energy exchanges (not shown). For large Stokes numbers, an alternative second-order ACBMM using transport equations for the RUM stresses should be adopted.

7. Conclusion

An algebraic-closure-based moment method has been developed for unsteady Eulerian particle simulations coupled with DNS of turbulent flows in very dilute regime and up to large Stokes numbers St_K (based on the Kolmogorov timescale) or moderate

Stokes numbers St (based on the turbulent macroscale seen by the particles). It relies on a conditional statistical approach (Février et al., 2005) which provides a local and instantaneous characterization of the dispersed-phase dynamic as it accounts for the effect of crossing between trajectories of inertial particles. ACBMM entails the numerical integration of a set of closed equations describing the evolution of the low-order moments of the conditional PDF, namely the mesoscopic particle number density and the mesoscopic particle velocity. Closures for the second-order velocity correlation, the RUM particle kinetic stress tensor, appearing in the particle momentum equation, are provided by means of an additional transport equation for the trace of the tensor and an algebraic closure for its deviatoric part. The ACBMM approach bases its efficiency and accuracy on such an algebraic closure; in this study, this concern has been addressed. The main results of the current study together with some important observations from previous analyses of the authors are summarized below. In very dilute regime, the RUM stress tensor is found to behave, in principal axes, as in a one-component limit state (line shape) which means that the RUM agitation develops in one preferred direction while it is damped in the others. In turbulent fluid flows, the one-component limit is the long-time asymptotic solution provided by the rapid distortion theory (Rogers, 1991) of a HIT submitted to a strong shear. Then, a redistribution of energy between the stresses is ensured by the action of the pressure-strain correlations. It is conjectured that in very dilute regimes, where inter-particle collisions are negligible, the dispersed phase submitted to a strong shear develops anisotropy which achieves and preserves the theoretical asymptotic values of the one-component limit, as no redistribution between stresses is possible. For larger values of the solid volume fraction, the inter-particle collisions should lead to a return-to-isotropy mechanism similar to the pressure-strain correlation effect in turbulent fluid flows (Simonin, 1991b) and the dispersed phase should move away from the one-component limit state as the collision frequency increases. Such a high anisotropy arise some doubts about the legitimacy of a viscosity assumption based on the particle response time as a typical timescale. In kinetic theory of dilute gases this assumption, at the origin of the constitutive relation for Newtonian fluids, involves that the molecular motion adjusts rapidly to the change imposed by the local strain. Hence, for similarity, the basic assumption from which a particle-response-time-based viscosity model arises is violated when the ratio between the particle response time and the mesoscopic strain timescale, namely the Knudsen number, is large (i.e. $\tilde{\tau}_p S > 1$). This consideration motivated the authors to develop alternative linear and nonlinear algebraic closures based on the inverse of the particle rate-of-strain as a typical timescale. Moreover, since it was observed that in the dispersed phase it is frequent to have reverse energy exchanges, a positive and negative viscosities were also considered when developing alternative linear relationships. By this study, a variety of algebraic closures have been developed. It is apparent that the most fruitful are the explicit algebraic stress models (2ΦEASM) which are based on a self-similarity assumption of the RUM tensor and which use a polynomial representation for tensor functions. At the tensor level, they provide an excellent representation of the RUM tensor, almost independent of the particle inertia. However, the analysis performed at the scalar level, and based on the predictions of the RUM-kinetic-energy production, has pointed out as the accuracy of the models degenerates at large turbulent macroscale Stokes numbers ($St > 3$) in high shear zones of the jet. The term responsible for the energy exchange between contributions and identified as a production of the RUM kinetic energy, at large inertia and in high shear zones of the jet, tends toward zero-mean values despite its high local magnitudes. For large Stokes numbers, when in the presence of a mean shear, this term changes its nature and alternative strategies of modeling should be adopted. For such particle inertia, the limits pointed out by a first-order ACBMM could be overcame by a second-order ACBMM using transport equations of the RUM stresses.

Recently Balachandar (2009) and Balachandar and Eaton (2010) provided a schematic representation of the different approaches which may be employed in DNS/LES of multiphase flows. In DNS, they used the Kolmogorov timescale in order to separate the range of applicability of the different approaches, suggesting that the existing particle Eulerian models may provide effective predictions up to St_K of the order of unity. With restriction to the regime considered in this study and for the relatively low Reynolds-number simulations carried out, the present work has shown that using an ACBMM approach with an adequate closure for the RUM kinetic stress tensor, the range of applicability of the Eulerian approaches may be extended up to turbulent-macroscale Stokes numbers, St, of the order of unity (i.e. large Stokes numbers based on the Kolmogorov timescale or moderate turbulent-macroscale Stokes numbers). Further questions on the constitutive relation as, for example, indifference from the reference frame and realizability are left as a future work.

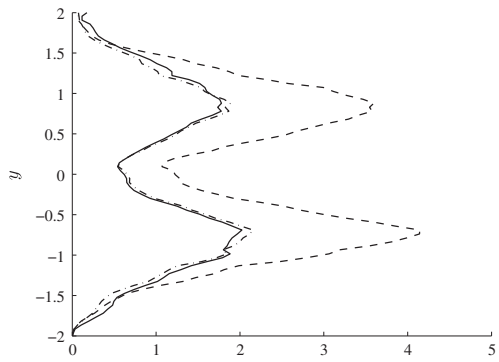

Fig. B.14. Particle–particle and particle–fluid fluctuating-velocity correlations computed from Lagrangian data (x10^{-4}). Solid line: $\langle w'_p w'_p \rangle_{xz}$, dash-dotted line: $\langle w'_{f@p} w'_p \rangle_{xz}$, dashed line: $\langle w'_{f@p} w'_{f@p} \rangle_{xz}$, for the 128^3 DNS of reference ($St \sim 1$), at the time $t = 6.2T^r_{f@p}$.

Acknowledgments

The authors wish to dedicate the manuscript to Professor Leonid I. Zaichik, Head of the Laboratory of Theoretical Heat and Hydrodynamics at the Institute for Safety Development of the Atomic Energy of the Russian Academy of Sciences, who died on December 3rd, 2010. Professor Zaichik contributed to this work with suggestions and fruitful discussions. His kindness and generosity as a man and his great expertise as a scientist will not be forgotten. He will remain a source of inspiration for all of us. An obituary of Professor Zaichik may be found in Reeks and Sommerfeld (2011).

This work received funding from the European Community through the TIMECOP-AE project (Project # AST5-CT-2006-030828). It reflects only the authors views and the Community is not liable for any use that may be made of the information contained therein. Numerical simulations were performed by the IBM Power6 machine; support of Institut de Développment et des Ressources en Informatique Scientifique (IDRIS) is gratefully acknowledged.

Appendix A. The Lagrangian approach for the particulate phase

The behavior of the particles interacting with the turbulence is investigated by the integration of the Newton equations corre-

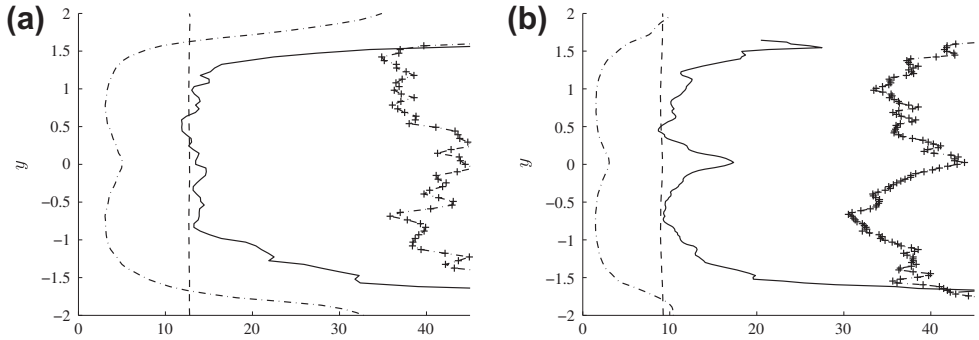

Fig. B.15. Timescales corresponding to (a) the 128^3 DNS of reference ($St \sim 1$) and (b) the 256^3 DNS. Dash-dotted line: τ_k, dashed line: τ^F_{fp}, solid line: $T_{f@p}$ and line with symbols: T_E, at the time $t = 6.2T^r_{f@p}$.

Table B.5
Mean particle relaxation times, turbulent-macroscale Stokes numbers and Kolmogorov Stokes numbers, at the time $t = 6.2T^r_{f@p}$.

DNS	128^3								256^3
τ^F_{fp}	1.3	6.4	12.7	25.4	38	63.2	88.4	126.1	9.1
St	∼0.1	∼0.5	∼1	∼2	∼3	∼5	∼7	∼10	1
St_K	∼0.4	∼2	∼4	∼8	∼12	∼20	∼28	∼40	6

sponding to the particle position and velocity. When the mixture is composed of spherical, rigid, non-rotating and non-interacting heavy particles with a diameter smaller or equal than the Kolmogorov lengthscale, the equations are strongly simplified since many contributions may be neglected. According to the studies of Maxey and Riley (1983) and Gatignol (1983), assuming no gravity, the equations governing the motion of each particle are written

$$\frac{\mathrm{d}\mathbf{x}_p}{\mathrm{d}t} = \boldsymbol{v}_p, \quad \frac{\mathrm{d}\boldsymbol{v}_p}{\mathrm{d}t} = -\frac{1}{\tau_p}(\boldsymbol{v}_p - \mathbf{u}_{f@p}), \tag{A.1}$$

where $\mathbf{u}_{f@p}(t) = \mathbf{u}_f(\mathbf{x}_p(t), t)$ is the undisturbed fluid velocity at the particle centre location and $\tau_p = (4\rho_p\, d_p)/(3\rho_f C_D\|\boldsymbol{v}_p - \mathbf{u}_{f@p}\|)$ is the particle response time. It accounts for the non-linearities of the drag force by means of the drag-coefficient correction as suggested by Schiller and Nauman (1935), $C_D = \frac{24}{Re_p}\left(1 + 0.15Re_p^{0.687}\right)$, formulated in terms of the particle Reynolds number $Re_p = (\|\boldsymbol{v}_p - \mathbf{u}_{f@p}\|d_p)/\nu_f$; ν_f is the kinematic fluid viscosity, ρ_f is the density of the fluid, ρ_p is the particle density and d_p is the particle diameter. The system of Eq. (A.1) is one-way coupled with an evolving turbulent flow which is exactly resolved by using the DNS approach.

Appendix B. Estimate of the particle Stokes number

The Stokes number is computed over a characteristic timescale of the turbulence seen by the particles, $T_{f@p}$, which is estimated from the Tchen equilibrium in the spanwise direction of the jet, mean-flow free. In this direction, when the well-known relations

$$\langle w'_p w'_p\rangle_{xz} \simeq \langle w'_{f@p} w'_p\rangle_{xz} \simeq \frac{T_{f@p}}{\tau^F_{fp} + T_{f@p}}\langle w'_{f@p} w'_{f@p}\rangle_{xz} \tag{B.1}$$

are attained (Prevost et al., 1996), the characteristic timescale $T_{f@p}$ may be deduced. w'_p is the particle velocity fluctuation obtained subtracting from any particle velocity the mean particle velocity computed using Lagrangian values averaged over xz-planes of one cell height; $w'_{f@p}$ is the fluid velocity fluctuation at the particle location. Correlations are then averaged over the same xz-planes. As an example, Fig. B.14 shows the mean particle–particle and particle–fluid correlation velocities used in (B.1), corresponding to one of the eight 128^3 DNSs (which is referred to as the reference). Results of Fig. B.14 show the validity of the relations (B.1) which therefore entails an accurate estimate of $T_{f@p}$. This simulation was chosen as a reference because it led to values of $T_{f@p}$ almost constant along the normal direction. Such results are depicted in Fig. B.15 together with the results of the 256^3 DNS. Mean relaxation times, Kolmogorov timescales and dissipation timescales are also shown for a comparison purpose. The estimate $T_{f@p}$ of the simulation of reference (i.e. $T^r_{f@p}$) was then used to evaluate the Stokes numbers of the other seven 128^3 DNSs. Indeed, in these simulations, the particle-to-gas density ratio is the only parameter modified in order to obtain different Stokes numbers. Moreover, as the particle diameter is small (see Section 5), the particle Reynolds number is such that the effect

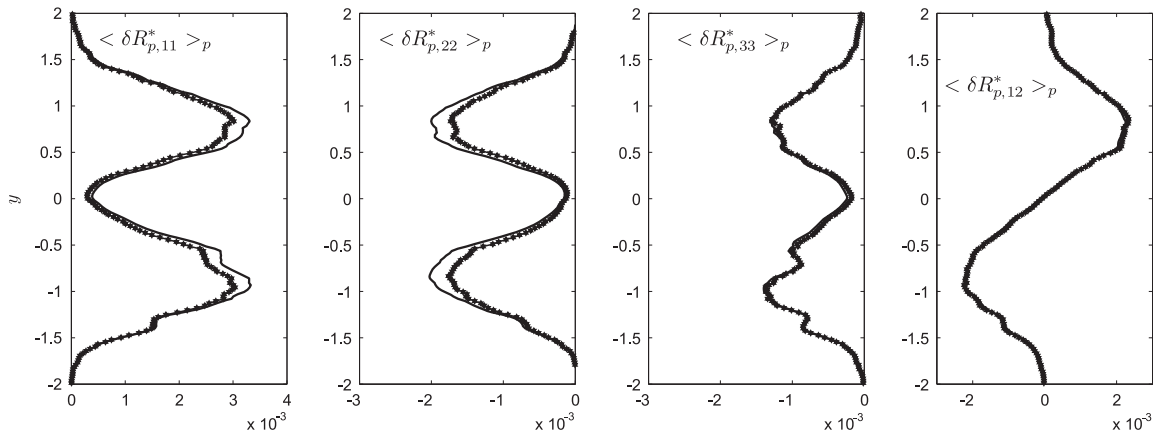

Fig. C.16. Profiles of actual (solid line) and modeled by 2ΦEASM2-C (line with symbols) deviatoric RUM stresses, corresponding to the 256^3 DNS ($St \sim 1$), at the time $t = 6\,T_{f@p}$.

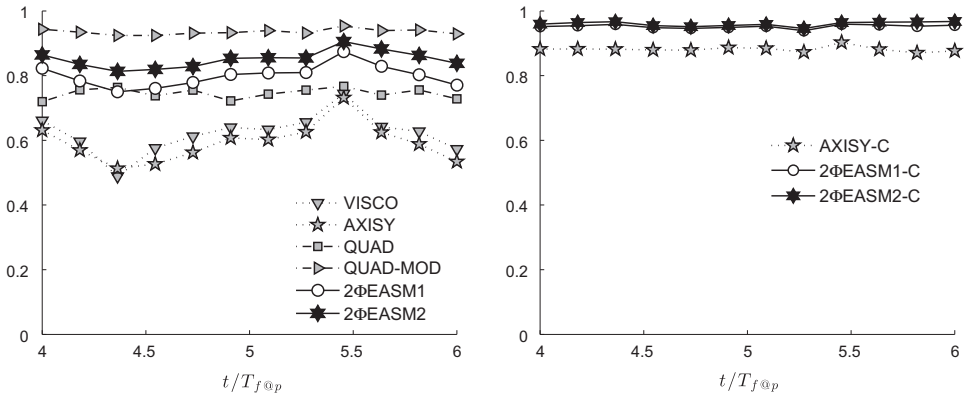

Fig. C.17. Correlation coefficients between the actual and the modeled scalar quantity P^*_{RUM}, at the periphery of the jet.

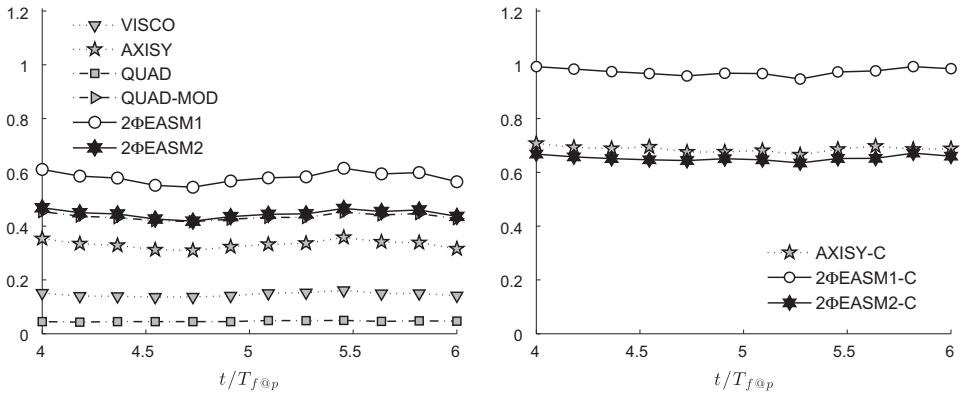

Fig. C.18. Magnitude ratios between the mean actual and the mean modeled scalar quantity P^*_{RUM}, at the periphery of the jet.

of the drag-coefficient correction on the particle response time is negligible. Using $T_{f@p}$, a turbulent-macroscale Stokes number is defined as $St = \tau^F_{fp}/T_{f@p}$ where $\tau^F_{fp} =< 1/\tau_p >^{-1}_{xz}$. A summary of the mean relaxation times and Stokes numbers characterizing the numerical simulations conducted in this study is given in Table B.5. For a comparison purpose, Stokes numbers based on the Kolmogorov timescale, $St_K = \tau^F_{fp}/\tau_K$, are also given. For timescales varying in the normal direction (as the Kolmogorov one), Stokes numbers are intended at the periphery of the jet.

Appendix C. Higher Reynolds number model assessment

The higher-Reynolds-number particle-laden slab (256^3 DNS) corresponds to a Stokes number $St \sim 1$. According to the analysis presented in Section 6, the assessment for this particle inertia may be performed indifferently using $\tilde{n}_p P^{*\prime}_{RUM}$ and $\tilde{n}_p P^*_{RUM}$, since they give similar results for $St \sim 1$. For this reason, at the scalar level, only the latter will be evaluated. At the tensor level, for sake of brevity, only the predictions of 2ΦEASM2-C are shown. Mean profiles of the deviatoric RUM are displayed in Fig. C.16. Results indicate a very good agreement between actual and modeled quantities, as expected. Fig. C.17 shows the correlations coefficients computed using all the models, with and without correction, over $\tilde{n}_p P^*_{RUM}$. Fig. C.18 shows the magnitude ratios between actual and modeled mean productions $< P^*_{RUM} >_p$. These results are consistent with the outcomes from the equivalent lower Reynolds number simulation ($St \sim 1$), both from a qualitative and from a quantitative viewpoint. Excellent predictions are provided using the 2ΦEASM models at this Stokes number. However, in Section 6.3 it has been shown that the models 2ΦEASM1/-C tend to underestimate the stress components. For this reason, 2ΦEASM2 (with or without correction) should be preferred.

References

Balachandar, S., 2009. A scaling analysis for point-particle approaches to turbulent multiphase flows. Int. J. Multiphase Flow 35, 801–810.

Balachandar, S., Eaton, J.K., 2010. Turbulent dispersed multiphase flow. Ann. Rev. Fluid Mech. 42, 111–133.

Balzer, G., Simonin, O., Boelle, A., Laviéville, J., 1996. A unifying modelling approach for the numerical prediction of dilute and dense gas-solid two-phase flows. In: Kwauk, M., Li, J. (Eds.), Circulating Fluidized Bed Technology V, Proc. of the 5th Int. Conf. on Circulating Fluidized Beds. Science Press, Beijing, pp. 432–439.

Batchelor, G.K., 1946. The theory of axisymmetric turbulence. Proc. Roy. Soc. Lond. Ser. A, Math. Phys. Sci. 186, 480–502.

Bhatnagar, P.L., Gross, E.P., Krook, M., 1954. A model for collision processes in gases. I. Small amplitude processes in charged and neutral one component systems. Phys. Rev. 94, 511525.

Chalons, C., Kah, D., Massot, M., 2012. Beyond pressureless gas dynamics: quadrature-based velocity moment models. Commun. Math. Sci. 10, 1241–1272.

Chandrasekhar, S., 1950. The theory of axisymmetric turbulence. Philos. Trans. Roy. Soc. Lond. Ser. A, Math. Phys. Sci. 242, 557–577.

Chapman, S., Cowling, T., 1939. The Mathematical Theory of Non-Uniform Gases, Cambridge Mathematical Library, Digital Reprint 1999 Edition. Cambridge University Press.

Chen, C.P., Wood, P.E., 1985. A turbulence closure model for dilute gas-particle flows. Can. J. Chem. Eng. 63, 349–360.

Chen, H., Orszag, S.A., Staroselsky, I., Succi, S., 2004. Expanded analogy between Boltzmann kinetic theory of fluids and turbulence. J. Fluid Mech. 519, 301–314.

Clark, R.A., Ferziger, J.H., Reynolds, W.C., 1979. Evaluation of subgrid-scale models using an accurately simulated turbulent flow. J. Fluid Mech. 91, 1–16.

Desjardins, O., Fox, R.O., Villedieu, P., 2008. A quadrature-based moment method for dilute fluid–particle flows. J. Comput. Phys. 227, 2514–2539.

Deutsch, E., Simonin, O., 1991. Large eddy simulation applied to the motion of particles in stationary homogeneous fluid turbulence. In: Turbulence Modification in Multiphase Flow, vol. 110. ASME FED, pp. 35–42.

Druzhinin, O.A., 1995. On the 2-way interaction in 2-dimensional particle-laden flows – the accumulation of particles and flow modification. J. Fluid Mech. 297, 49–76.

Druzhinin, O.A., Elghobashi, S., 1998. Direct numerical simulations bubble-laden turbulent flows using the two-fluid formulation. Phys. Fluids 10, 685–697.

Druzhinin, O.A., Elghobashi, S., 1999. On the decay rate of isotropic turbulence laden with microparticles. Phys. Fluids 11, 602–610.

Elghobashi, S.E., Abou-Arab, T.W., 1983. A two-equation turbulence model for two-phase flows. Phys. Fluids 26, 931–938.

Falkovich, G., Fouxon, A.S., Stepanov, M.G., 2002. Acceleration of rain initiation by cloud turbulence. Nature 419, 151–154.

Ferry, J., Balachandar, S., 2001. A fast Eulerian method for dispersed two-phase flow. Int. J. Multiphase Flow 27, 1199–1226.

Février, P., Simonin, O., Squires, K.D., 2005. Partitioning of particle velocities in gas–solid turbulent flows into a continuous field and a spatially uncorrelated random distribution: theoretical formalism and numerical study. J. Fluid Mech. 533, 1–46.

Fox, R.O., 2008. A quadrature-based third-order moment method for dilute gas-particle flows. J. Comput. Phys. 227, 6313–6350.

Fox, R.O., 2012. Large-eddy-simulation tools for multiphase flows. Ann. Rev. Fluid Mech. 44, 47–76.

Fox, R., Laurent, F., Massot, M., 2008. Numerical simulation of spray coalescence in an Eulerian framework: direct quadrature method of moments and multi-fluid method. J. Comput. Phys. 227, 3058–3088.

Gatignol, R., 1983. The Faxen formulae for a rigid particle in an unsteady non uniform Stokes flow. J. Mech. Theor. Appl. 9, 143–160.

Gatski, T.B., Speziale, C.G., 1993. On explicit algebraic stress models for complex turbulent flows. J. Fluid Mech. 254, 59–78.

Gatski, T.B., Wallin, S., 2004. Extending the weak-equilibrium condition for algebraic Reynolds stress models to rotating and curved flows. J. Fluid Mech. 518, 147–155.

Gidaspow, D., 1994. Multiphase Flow and Fluidization: Continuum and Kinetic Theory Descriptions. Academic Press.

Girimaji, S.S., 1996. Fully explicit and self-consistent algebraic Reynolds stress model. Theor. Comput. Fluid Dyn. 8, 387–402.

Girimaji, S.S., 1997a. A Galilean invariant explicit algebraic Reynolds stress model for turbulent curved flows. Phys. Fluids 9, 1067–1077.

Grad, H., 1949. On the kinetic theory of rarefied gases. Commun. Pure Appl. Math. 2, 331–407.

Grundestam, O., Wallin, S., Johansson, A.V., 2005. Techniques for deriving explicit algebraic Reynolds stress models based on incomplete sets of basis tensors and predictions of fully developed rotating pipe flow. Phys. Fluids 17, 115103.

Gustavsson, K., Meneguz, E., Reeks, M., Mehlig, B., 2012. Inertial-particle dynamics in turbulent flows: caustics, concentration fluctuations, and random uncorrelated motion. New J. Phys. 14, 115017.

Higgins, C., Parlange, M.B., Meneveau, C., 2003. Alignment trends of velocity gradients and subgrid-scale fluxes in the turbulent atmospheric boundary layer. Bound. Lay. Meteorol. 109, 59–83.

IJzermans, R.H.A., Meneguz, E., Reeks, M.W., 2010. Segregation of particles in incompressible random flows: singularities, intermittency and random uncorrelated motion. J. Fluid Mech. 653, 99–136.

Jongen, T., Gatski, T., 1998. General explicit algebraic stress relations and best approximation for three-dimensional flows. Int. J. Eng. Sci. 36, 739–763.

Jovanović, J., Otić, I., 2000. On the constitutive relation for the Reynolds stresses and the Prandtl–Kolmogorov hypothesis of effective viscosity in axisymmetric strained turbulence. J. Fluids Eng. 122, 48–50.

Kah, D., Laurent, F., Fréret, L., de Chaisemartin, S., Fox, R.O., Reveillon, J., Massot, M., 2010. Eulerian quadrature-based moment models for dilute polydisperse evaporating sprays. Flow, Turbul. Combust. 85, 649–676.

Kaufmann, A., Moreau, M., Simonin, O., Helie, J., 2008. Comparison between Lagrangian and mesoscopic Eulerian modelling approaches for inertial particles suspended in decaying isotropic turbulence. J. Comput. Phys. 227, 6448–6472.

Laurent, F., Massot, M., 2001. Multi-fluid modeling of laminar poly-dispersed spray flames: origin, assumptions and comparison of sectional and sampling methods. Combust. Theor. Model. 5, 537–572.

Lele, S., 1992. Compact finite difference schemes with spectral like resolution. J. Comput. Phys. 103, 16–42.

Lumley, J.L., 1978. Computational modeling of turbulent flows. Adv. Appl. Mech. 18, 123–176.

Lund, T.S., Rogers, M.M., 1994. An improved measure of strain state probability in turbulent flows. Phys. Fluids 6, 1838–1847.

Marchisio, D.L., Fox, R.O., 2005. Solution of population balance equations using the direct quadrature method of moments. J. Aerosol Sci. 36, 43–73.

Masi, E., Riber, E., Sierra, P., Simonin, O., Gicquel, L.Y.M., 2010. Modeling the random uncorrelated velocity stress tensor for unsteady particle Eulerian simulation in turbulent flows. In: Proceedings of the 7th International Conference on Multiphase Flow (ICMF). Tampa, Florida, May 30–June 4.

Masi, E., Simonin, O., Bédat, B., 2011. The mesoscopic Eulerian approach for evaporating droplets interacting with turbulent flows. Flow, Turbul. Combust. 86, 563–583.

Maxey, M.R., 1987. The gravitational settling of particles in homogeneous turbulence and random flow. J. Fluid Mech. 26, 441.

Maxey, M.R., Riley, J.J., 1983. Equation of motion for a small rigid sphere in a non uniform flow. Phys. Fluids 26, 2883–2889.

McGraw, R., 1997. Description of aerosol dynamics by the quadrature method of moments. Aerosol Sci. Technol. 27, 255–265.

Meneguz, E., Reeks, M.W., 2011. Statistical properties of particle segregation in homogeneous isotropic turbulence. J. Fluid Mech. 686, 338–351.

Moreau, M., 2006. Modélisation numérique directe et des grandes échelles des écoulements turbulents gaz-particules dans le formalisme Eulérien mésoscopique. Ph.D. thesis, Institut National Polytechnique de Toulouse.

Moreau, M., Simonin, O., Bédat, B., 2010. Development of gas–particle Euler–Euler LES approach: a priori analysis of particle sub-grid models in homogeneous isotropic turbulence. Flow, Turbul. Combust. 84, 295–324.

Passalacqua, A., Fox, R.O., Garg, R., Subramaniam, S., 2010. A fully coupled quadrature-based moment method for dilute to moderately dilute fluid–particle flows. Chem. Eng. Sci. 65, 2267–2283.

Passot, T., Pouquet, A., 1987. Numerical simulation of homogeneous flows in the turbulent regime. J. Fluid Mech. 181, 441.

Pope, S.B., 1975. A more general effective-viscosity hypothesis. J. Fluid Mech. 72, 331–340.

Prevost, F., Boree, J., Nuglisch, H.J., Charnay, G., 1996. Measurements of fluid/particle correlated motion in the far field of an axisymmetric jet. Int. J. Multiphase Flow 22, 685–701.

Rani, S.L., Balachandar, S., 2003. Evaluation of the equilibrium Eulerian approach for the evolution of particle concentration in isotropic turbulence. Int. J. Multiphase Flow 29, 1793–1816.

Reeks, M.W., 1991. On a kinetic equation for the transport of particles in turbulent flows. Phys. Fluids 3, 446–456.

Reeks, M., Sommerfeld, M., 2011. L. I. Zaichik, 1947–2010. Int. J. Multiphase Flow 37, 235.

Riber, E., 2007. Développement de la méthode de simulation aux grandes échelles pour les écoulements diphasiques turbulents. PhD thesis, Institut National Polytechnique de Toulouse.

Riber, E., Moureau, V., García, M., Poinsot, T., Simonin, O., 2009. Evaluation of numerical strategies for large eddy simulation of particulate two-phase recirculating flows. J. Comput. Phys. 228, 539–564.

Riley, J.J., Paterson, G.S., 1974. Diffusion experiments with numerically integrated isotropic turbulence. Phys. Fluids 17, 292–297.

Rodi, W., 1972. The prediction of free turbulent boundary layers by use of a two-equation model of turbulence. Phd thesis, University of London.

Rodi, W., 1976. A new algebraic relation for calculating the Reynolds stresses. Z. Angew. Math. Mech. 56, 219–221.

Rogers, M.M., 1991. The structure of a passive scalar field with a uniform mean gradient in rapidly sheared homogeneous turbulent flow. Phys. Fluids A: Fluid Dyn. 3, 144–154.

Rotta, J., 1951. Statistische theorie nichthomogener turbulenz.I. Z. Phys. 129, 547–572.

Sakiz, M., Simonin, O., 1999. Numerical experiments and modelling of non-equilibrium effects in dilute granular flows. In: Brun, R., Campargue, R., Gatignol, R., Lengrand, J.C. (eds.) Rarefied Gas Dynamics, Proceedings of the 21st International Symposium on Rarefied Gas Dynamics, Cépadués Editions, vol. 1. Marseille (France), pp. 287–294.

Schiller, L., Nauman, A., 1935. A drag coefficient correlation. V.D.I. Zeit. 77, 318–320.

Shotorban, B., Balachandar, S., 2006. Particle concentration in homogeneous shear turbulence simulated via Lagrangian and equilibrium Eulerian approaches. Phys. Fluids 18, 065105.

Simonin, O., 1991a. Prediction of the dispersed phase turbulence in particle-laden jets. In: Proceedings of the 4th International Symposium on Gas–Solid Flows, vol. 121. ASME FED, pp. 197–206.

Simonin, O., 1991b. Second-moment prediction of dispersed phase turbulence in particle-laden flows. In: Proceedings of the 8th Symposium on Turbulent Shear Flows, vol. 1. Munich, Federal Republic of Germany, pp. 741–746.

Simonin, O., 2000. Statistical and continuum modelling of turbulent reactive particulate flows. Part 1: Theoretical derivation of dispersed Eulerian modelling from probability density function kinetic equation. In: Lecture Series 2000–06. von Karman Institute for Fluid Dynamics.

Simonin, O., Février, P., Laviéville, J., 2002. On the spatial distribution of heavy particle velocities in turbulent flow: from continuous field to particulate chaos. J. Turbul. 3, N40.

Simonin, O., Zaichik, L.I., Alipchenkov, V.M., Février, P., 2006. Connection between two statistical approaches for the modelling of particle velocity and concentration distributions in turbulent flow: the mesoscopic Eulerian formalism and the two-point probability density function method. Phys. Fluids 18, 125107.

Spencer, A.J.M., 1971. Theory of invariants. In: Eringen, A.C. (Ed.), Continuum Physics, vol I part III. Academic Press, New-York.

Speziale, C.G., Xu, X.-H., 1996. Towards the development of second-order closure models for nonequilibrium turbulent flows. Int. J. Heat Fluid Flow 17, 238–244.

Tao, B., Katz, J., Meneveau, C., 2002. Statistical geometry of subgrid-scale stresses determined from holographic particle image velocimetry measurements. J. Fluid Mech. 457, 35–78.

Taulbee, D.B., 1992. An improved algebraic stress model and corresponding nonlinear stress model. Phys. Fluids A 4, 2555–2561.

Vance, M.W., Squires, K.D., Simonin, O., 2006. Properties of the particle velocity field in gas-solid turbulent channel flow. Phys. Fluids 18, 13.

Vermorel, O., Bédat, B., Simonin, O., Poinsot, T., 2003. Numerical study and modelling of turbulence modulation in a particle laden slab flow. J. Turbul. 4, N25.
Vié, A., Chalons, C., Fox, R., Laurent, F., Massot, M., 2011. A multi-Gaussian quadrature method of moments for simulating high stokes number turbulent two-phase flows. Ann. Res. Briefs CTR, 309–320.
Wallin, S., Johansson, A.V., 2000. An explicit algebraic Reynolds stress model for incompressible and compressible turbulent flows. J. Fluid Mech. 403, 89–132.
Wallin, S., Johansson, A.V., 2002. Modelling streamline curvature effects in explicit algebraic Reynolds stress turbulence models. Int. J. Heat Fluid Flow 23, 721–730.
Weis, J., Hutter, K., 2003. On Euclidean invariance of algebraic Reynolds stress models in turbulence. J. Fluid Mech. 476, 63–68.
Yuan, C., Fox, R., 2011. Conditional quadrature method of moments for kinetic equations. J. Comput. Phys. 230, 8216–8246.
Zaichik, L.I., 1999. A statistical model of particle transport and heat transfer in turbulent shear flows. Phys. Fluids 11, 1521–1534.
Zaichik, L.I., 2009. A quadratic algebraic approximation of the RUV second-order moment. Pers. Commun..
Zaichik, L.I., Vinberg, A.A., 1991. Modelling of particle dynamics and heat transfer in turbulent flows using equations for first and second moments of velocity and temperature fluctuations. In: Proceedings of the 8th Symposium on Turbulent Shear Flows, vol. 1. Munich, Federal Republic of Germany, pp. 1021–1026.
Zaichik, L.I., Simonin, O., Alipchenkov, V.M., 2003. Two statistical models for predicting collision rates of inertial particles in homogeneous isotropic turbulence. Phys. Fluids 15, 2995–3005.
Zhou, L.X., 2010. Advances in studies on two-phase turbulence in dispersed multiphase flows. Int. J. Multiphase Flow 36, 100–108.